NASA CR-132324

NYU-AA-72-27

NEW YORK UNIVERSITY
SCHOOL OF ENGINEERING AND SCIENCE
DEPARTMENT OF AERONAUTICS AND ASTRONAUTICS

ANALYSIS OF AN ENTRAINMENT MODEL OF THE JET IN A CROSSFLOW

H.S. CHANG

and

J.E. WERNER

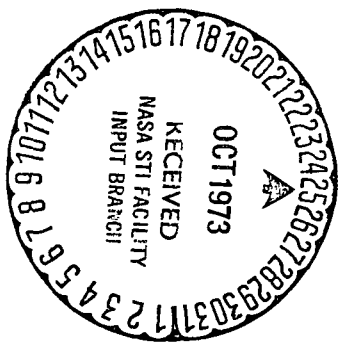

Prepared for the
National Aeronautics and Space Administration
under research grant NGR-33-016-141

FOREWORD

This report was prepared by Dr. Jack Werner, Associate Professor of Aeronautics and Astronautics, and Mr. H S Chang, Graduate Research Assistant in the Department of Aeronautics and Astronautics.

The research has been carried out under NASA Grant NGR-33-016-141 under the technical cognizance of Mr. Richard Margason.

ABSTRACT

A theoretical model has been proposed for the problem of a round jet in an incompressible cross-flow. The method of matched assymptotic expansions has been applied to this problem. Inner and outer expansions have been obtained in terms of the expansion parameter $\epsilon = R_{jo}/r_t$ where R_{jo} is the jet orifice radius and r_t is the minimum radius of curvature of the jet trajectory. For the solution to the flow problem in the inner region, the re-entrant wake flow model was used with the re-entrant flow representing the fluid entrained by the jet. Higher order corrections are obtained in terms of this basic solution. The perturbation terms in the outer region was found to be a line distribution of doublets and sources. The line distribution of sources represents the combined effect of the "entrainment" and the "displacement". For large values of U_∞/U_j, the effect of the "entrainment" is small while the effect of the "displacement" is important. For small value of U_∞/U_j, the opposite is true. Pressure coefficient contours for $U_j/U_\infty = .25$, .5, and .8 were computed for inner and outer region. The variation of jet radius, source strength, and mean jet velocity as functions of distance along the jet trajectory were also computed to aid in assessing the role of these quantities in the interaction.

TABLE OF CONTENTS

LIST OF FIGURES

LIST OF SYMBOLS

A_1, A_3, b, c, d	Five constants which determine the characteristics of the Re-entrant Flow Model, see Section (V-e)
a_m, b_o, $m \geq 0$	Coefficient of power series expansion of $W_2(Z,s)$ see equ. (V-36)
C_P	Pressure coefficient
D(s)	Total drag at s
$D_2(s)$	Drag of Re-entrant Flow Model
E(s)	Total entrainment per unit length of jet at s
$E_2(s)$	Entrainment of Re-entrant Flow Model
$\bar{e}_X$, $\bar{e}_Y$, $\bar{e}_s$	Unit vector in x_1, y_1, s_1 direction (curvalinear coordinate)
$f_m(\epsilon)$	Coefficient of m^{th} term outer expansion
$g_m(\epsilon)$	Coefficient of m^{th} term inner expansion
$G_i(s)$	A function defined by equ. (V-6b)
$\bar{i}$, $\bar{j}$, $\bar{k}$	Unit vector in x_{1_o}, y_{1_o}, Z_{1_o} direction (Cartesian coordinate)
$m_j(S)$	Mass flux through jet cross-section at S
$M_j(S)$	Momentum flux through jet cross-section at S
$\bar{n}$	Unit normal vector to σ
$P_w(s_1)$	Wake pressure of Re-entrant Flow Model
P_∞	Cross-flow pressure at infinity
P_n	n^{th} order Lagrangian Polynomial
$P_i(s)$	A function defined by equ. (V-5b)
$\bar{q}$	Velocity vector of cross-flow
r_t	Minimum radius of curvature of jet trajectory
$r_1(s)$	Radius of curvature of jet trajectory at s_1
r_o	Distance between a singularity and the point where the potential due to this singularity is evaluated

$R_{j_1}(s_1)$	Radius of curvature of σ_j at s_1
R_{jo}	Radius of jet orifice
$R_j(s)$	$R_{j1}(s_1)/R_{jo}$
R_o	r_o/ϵ
s_1	Distance along jet trajectory
s	s_1/r_t
S	s_1/R_{jo}
$T_1(s)$	A function defined by equ. (V-5a)
U_∞	Undisturbed cross-flow velocity
U_n	Component of U_∞ normal to jet trajectory
U_j	Jet velocity at jet orifice
U_w	Velocity of the streamline BHFE (Fig. 4) $(1 - Q)^{\frac{1}{2}}$
$V_j(S)$	Average jet velocity at S (Fig. 11)
$W_a(Z.s)$	Complex potential of Re-entrant Flow Model
x,y	x_1/r_t, y_1/r_t
X,Y	x_1/R_{jo}, y_1/R_{jo}
x_1, y_1	Coordinate normal to jet trajectory at s_1 (Fig. 2)
x_{1o}, y_{1o}	Coordinate in jet orifice plate (Fig. 2)
x_o, y_o	x_{1o}/r_t, y_{1o}/r_t
X_o, Y_o	x_{1o}/R_{jo}, y_{1o}/R_{jo}
z	Complex variable $x + iy$
Z	Complex variable $X + iY$
z_{1o}	Coordinate normal to the orifice plate
z_o	z_{1o}/r_t
Z_o	z_{1o}/R_{jo}
α	Angle of jet trajectory with respect to x_{1o} axis (Fig. 2)

γ	Angle between singularity axis and displacement vector $\bar{r}_o$ (Fig. 3)
$\gamma(\epsilon)$	A function ϵ only, used to compare order of magnitude in asymptotic expansion
ϵ	R_j/r_t
Φ	Velocity potential
φ	Dimensionless potential $\Phi/U_\infty r_t$
$\mu_o^1, \mu_o^{(i)}$	Three-dimensional source strength for i^{th} order outer solution
$\mu_1^i, \mu_o^{(i)}$	Three-dimensional doublet strength for i^{th} order outer solution
ρ_∞	Cross-flow density
ρ_j	Jet density
Ψ	Dimensionless stream function
$(\ )^i$	Inner region
$(\ )^o$	Outer region
$[(\ )^i]_o$	Asymptotic behavior at outer limit of inner region
$[(\ )^o]_i$	Asymptotic behavior at inner limit of outer region
σ	Boundary streamline of Re-entrant Flow Model (Fig. 4)

I. INTRODUCTION

One of the methods currently employed to achieve vertical take-off performance in VTOL aircraft is to install a lifting jet. An inherent problem of such an installation is that it interacts with the crossflow due to horizontal flight resulting in an induced flow field which has a measurable influence on flight characteristics.

In recent years, considerable amount of attention has been paid to this field. In the experimental area, Jordinson, Ref. [8] made pressure measurements in the jet plume which gave jet penetration data and the total pressure contours. Later, Bradbury and Wood, Ref. [7], and Vogler, Ref. [9], measured the pressure distribution on the orifice plate of the jet. Recently, Mosher, Ref. [2], weighed the relative importance of the effect of blockage and the effect of entrainment on the induced flow at various ratios of jet exit velocity to free cross-flow velocity, i.e., U_j/U_∞. The most extensive wind-tunnel tests were done by Fricke, Wooler and Ziegler, Ref. [1]. They obtained data not only for a one jet configuration, but also for two and three jet configurations.

One of the most comprehensive descriptions of the jet in a cross-flow was given by Keffer and Baines, Ref. [3]. The picture which emerges from their work is of a jet initially comprised of a potential core surrounded by a growing turbulent shear region. Within a few diameters of the orifice, the jet is completely turbulent, its cross-section becoming kidney-shaped and finally developing the appearance of two counter rotating vortices far downstream. Over the initial stages of the jet, the cross-flow is described as separating from the jet somewhere near the widest point of its cross-section. A "wake" region immediately behind the jet is characterized by negative pressure coefficients in contrast to the upstream face where pressure coefficients

become positive. The initial bending of the jet is ascribed to this pressure "defect" in the wake. Further along the jet axis beyond the potential core stage, the jet is described as fully developed or "established" and some tendency toward similarity is noted in the velocity profiles measured by Keffer and Baines. The pressure differences in front of and behind the jet diminish and the bending of the jet is ascribed mainly to the shear stress and momentum exchange due to turbulent mixing or entrainment.

Among the initial analytical efforts were attempts by Shandorov and others, Ref. [12], to derive the jet trajectory. Margason, Ref. [10] has proposed an empirically derived equation developed by matching experimental data. The results of these investigations have been used by Rubbert, Ref. [11] to provide the trajectory at the outset thus reducing the problem to a fixed rather than a free boundary one. While Rubbert solves the three-dimensional problem completely by computer methods, his potential model contains no mechanism to account for the bending of the jet according to the assumed shape. Wooler, Ref. [5], actually does derive the jet trajectory, introducing entrainment parameter and a drag coefficient in the process. These are evaluated by fitting his derived trajectory to Margason's curve. With the trajectory so determined, he uses a line distribution of doublets along the trajectory to simulate the "local blockage" effect and a line distribution of sources to represent the effect of entrainment. This is the so-called sink-doublet model. However, this model provides no mechanism to account for the bending of the jet and the three-dimensional effect of the trajectory curvature on induced flow is neglected.

Werner and Chang, Ref. [4], solved a complete three-dimensional potential flow problem by dividing the flow field into inner and outer regions. Separate inner and outer solutions were found in each region and these two solutions

were matched by asymptotic expansion techniques in an intermediate region. For the inner solutiin, the first order term was found to be the locally two dimensional solution to flow about the jet cross-section. For this component, the Riabouchinsky wake flow model was adopted.

For the outer solution, the first perturbation was found to consist not only of the familiar doublet distribution but a source distribution as well. This latter distribution resulted from the displacement effect of the jet as turned in the downstream direction. As such, it had two components, one proportional to the trajectory curvature and a second contribution due to the increase in jet cross-sectional area. This result raised a rather fundamental question about the use of net sink distributions to represent entrainment effects: If the fluid entering the "sink" is to be considered a part of the jet, the jet displacement increases requiring an additional source term in the solution and the net sink strength should be zero.

The flow model of Werner and Chang, Ref. [4], did not consider explicitly the effect of entrainment by the jet. It's the purpose of this investigation to explore the analytical structure of a model in which the effects of entrainment, blockage and curvature exist concurrently. The particular model has been chosen largely an mathematical grounds and admittedly an element of artificiality has been introduced thereby. On the other,hand, it provides a framework in which to explore the mutual dependence of entrainment, trajectory curvature and blockage, while the resulting insight should be useful in the treatment of more rigorous models.

II. THE FLOW MODEL

The model to be used in this investigation together with pertinent coordinate systems are illustrated in Fig. 1 and Fig. 2. The external cross-flow is assumed to be steady and inviscid. A vortex sheet which encloses the whole jet is the inner boundary of this problem. The plane normal to the jet trajectory intersects the vortex sheet to give a shape shown in Fig. 4. For external cross-flow, this vortex sheet can be regarded as a streamline in the normal plane. The streamline (or vortex line) CABHF is assumed to separated from the jet at B, and a wake of constant pressure $Pw(s_1)$ is formed immediately behind the separation point. Then this streamline rolls-up, forms a backwards stream HH′FF′ at the center of the wake and flows into the jet. The backwards stream HH′FF′ is called reentrant flow.

The geometrical shape of the wake and flow-rate of the reentrant flow is governed by the cavity number Q and U_∞, where

$$Q = \frac{Pw - P_\infty}{\frac{1}{2} U_n^2 \rho} \tag{II-1}$$

$$U_n = U_\infty \sin\alpha \tag{II-2}$$

If Q is assumed constant along the jet trajectory, the shape in each normal plane will be geometrically similar. In this investigation, we do assume that Q is constant.

In each normal plane, the reentrant flow carries some fluids of external cross-flow and flows into the jet. Then, these fluids are carried away by the jet into the next normal plane and forms so called entrainment. Two assumptions have been implied here; all entrainment occurs in the wake and there will be no entrainment if the external cross-flow velocity is zero.

But from the study of Keffer and Bains (Ref. [3]), the entrainment of a jet in a cross-flow is much greater than that of a free jet. And, the backwards flow in the center of wake of jet is confirmed by Mosher (Ref. [2]). These assumptions might not be bad after all.

III. MATHEMATICAL FORMULATION

a) Formulation of the problem

Since the flow exterior to the vortex sheet (Fig. 1) is assumed to be inviscid and steady, a velocity potential Φ exists and is governed by Laplace's Equation. A boundary valued problem is thus formed as following:

$$\nabla^2 \Phi = 0 \qquad \text{(III-1)}$$

1. Inner Boundary Condition: On the vortex sheet the velocity vector is tangential to this sheet.
2. Outer Boundary Condition: At infinitely far away from the jet, the velocity vector is $U_\infty \bar{i}$.
3. On the plane $Z_{10} = 0$, the velocity vector is tangential to this plane.

b) Image System

The third boundary condition in preceding section is solved by reflecting the flow field into the lower half space (dotted line in Fig. 2). Now, the new flow field is symmetrical with respect to the plane $Z_{10} = 0$; the velocity on this plane is, therefore, tangential to this plane.

c) Inner and Outer Solution

The method of asymptotic expansion (Refs. [13, 14 and 15]) is used to solve the problem formulated in preceding sections. By this method, separated "inner" and "outer" solutions are introduced, with inner solution satisfying the inner boundary condition and outer solution satisfying the outer solution. In a intermediate region, these two solutions are matched asymptotically. Also, Laplace's Equation is satisfied by both inner and outer solutions. The use of this method is prompted by the fact that, due to three-dimensional nature of the problem and geomtrical complexity of the inner boun-

dary, it is extremely difficult to obtain an analytic solution which can be applied throughout the flow region. And also, for $U_\infty/U_j \ll 1$, the radius of curvature r_t of the jet will be large compared to the jet radius R_j, i.e., $R_{jo}/r_t \ll 1$. Under this condition, the flow near the jet, within a radius of the order of R_j, is expected to be nearly two-dimensional, but not completly so.

Introducing

$$\epsilon = \frac{R_{jo}}{r_t} \tag{III-2}$$

as a parameter, we write inner and outer solutions as asymptotic series:

$$\varphi^i(X,Y,s;\epsilon) \sim \sum_0^\infty g_m(\epsilon)\,\varphi_m^i(X,Y,s) \tag{III-3a}$$

with X,Y fixed as $\epsilon \to o$

$$\varphi^o(x,y,s;\epsilon) \sim \sum_0^\infty f_m(\epsilon)\,\varphi_m^o(x,y,s) \tag{III-3b}$$

with x,y fixed as $\epsilon \to o$

where

$$\varphi = \frac{\Phi}{U_\infty r_t} \quad \text{non-dimensional potential} \tag{III-4a}$$

$$X = \frac{x_1}{R_{jo}}\ ,\ Y = \frac{y_1}{R_{jo}}\ ,\ s = \frac{s_1}{r_t} \quad \text{non-dimensional inner variables} \tag{III-4b}$$

$$x = \frac{x_1}{r_t}\ ,\ y = \frac{y_1}{r_t}\ ,\ s = \frac{s_1}{r_t} \quad \text{non-dimensional outer variables} \tag{III-4c}$$

f_m's and g_m's are functions of the parameter ϵ only with the property:

$$\frac{f_{m+1}(\epsilon)}{f_m(\epsilon)} \to o \quad \text{as} \quad \epsilon \to o \tag{III-5}$$

Eq. (III-4) establishes R_{jo} as the basic normal length scale and r_t as the basic tangential (to the trajectory) scale for phenomenona in the inner region. The basic length scale in the outer region is r_t for every direction. At this point, attention should be called to the following fact:

$$\frac{\partial \Phi}{\partial x_1} \sim \frac{U_\infty}{\epsilon}\left[f_o(\epsilon)\frac{\partial \varphi_o^i}{\partial X} + \ldots.\right] = o\left[\frac{f_o(\epsilon)}{\epsilon}\right] \qquad \text{(III-6a)}$$

$$\frac{\partial \Phi}{\partial s_1} \sim U_\infty\left[f_o(\epsilon)\frac{\partial \varphi_o^i}{\partial s} + \ldots.\right] = o\left[f_o(\epsilon)\right] \qquad \text{(III-6b)}$$

If $f_o(\epsilon)$ is taken to be unit, which will not lose generality in comparing order of magnitude, then $\partial\Phi/\partial x_1$ is of order $(1/\epsilon)$, while $\partial\Phi/\partial s_1$ is of order (1). In other words, following important assumption is implied in this way of formulating inner and outer expansion; in inner region, variation in Φ for a displacement of $o(R_{jo})$ in X-Y plane are of the same order as variation for a displacement of $o(r_t)$ in s direction. This assumption is, of course, true as long as U_∞/U_j remains small.

d) Basic equation in dimensionless variables

As stated before, both inner and outer solution should satisfy Laplace equation. In inner region, Laplace's equation in inner variable takes the form (Ref. [4]).

$$\frac{\partial^2 \varphi^i}{\partial X^2} + \frac{\partial^2 \varphi^i}{\partial Y^2} - \frac{\epsilon\, h(s)}{1-\epsilon h X}\frac{\partial \varphi^i}{\partial X} + \epsilon^2\left[\frac{\partial \varphi^i}{\partial s}\frac{\partial}{\partial s}\left(\frac{1}{2(1-\epsilon h X)^2}\right) + \left(\frac{1}{1-\epsilon h X}\right)^2\frac{\partial^2 \varphi^i}{\partial s^2}\right] = 0 \qquad \text{(III-7)}$$

where

$$h(s) = r_t/r_1(s_1)$$

Expanding the coefficients into power series, Equ. (III-7) can be written as

$$\frac{\partial^2 \varphi^i}{\partial X^2} + \frac{\partial^2 \varphi^i}{\partial Y^2} - \epsilon\, h(s)\, \frac{\partial \varphi^i}{\partial X} + \epsilon^2 \left[\frac{\partial^2 \varphi^i}{\partial s^2} - h^2(s)\, X \frac{\partial \varphi^i}{\partial X} \right] + 0(\epsilon^3) \sim 0 \qquad \text{(III-8)}$$

Since the specific form of $g_m(\epsilon)$'s in Eq. (III-3a) is still unknown, we cannot substitute Eq. (III-3a) into (III-8) to obtain the governing equation for each φ_m^i's.

In outer region, the parameter ϵ does not appear explicitly in the Laplace Equation in outer variables. Thus, Equ. (III-3b) can be substituted into $\nabla^2 \varphi_o = 0$ to obtain the governing equation for each φ_m^o as:

$$\nabla^2 \varphi_m^o = 0 \quad , \quad \text{for } m \geq o \qquad \text{(III-9)}$$

where ∇^2 is the three-dimensional Laplacian.

e) Boundary conditions

If the vortex sheet (Fig. 1) is given by the equation,

$$F(x_1, y_1, s_1) = 0 \qquad \text{(III-10)}$$

the over-all inner boundary condition will take the form:

$$\nabla \varphi^i \cdot \nabla F = 0 \qquad \text{(III-11)}$$

But the inner boundary condition for each φ_m^i is yet unknown.

The over-all outer boundary condition is

$$\lim_{x,y \to \infty} \nabla \varphi^o = \bar{i} \qquad \text{(III-12)}$$

By substituting Eq. (III-3b) into this equation, the outer boundary condition for each φ_m^o are obtained

$$\lim_{x,y \to \infty} \nabla \varphi_o^o = \bar{i} \qquad \text{(III-13a)}$$

$$\lim_{x,y \to \infty} \nabla \varphi_m^o = 0 \ , \ \text{for } m \geq 1 \qquad \text{(III-13b)}$$

The remaining conditions are supplied by requiring the inner and outer solution to match asymptotically over an intermediate region. Formally, this can be stated as

$$\lim_{\epsilon \to o} \frac{\left[\sum_{o}^{M} g_m(\epsilon)\, \varphi_m^i\right]_o - \left[\sum_{o}^{N} f_n(\epsilon)\varphi_n^o\right]_i}{\gamma(\epsilon)} \sim 0 \qquad \text{(III-14)}$$

The notation $[\ \ ]_o$ denotes behavior near the outer bound of the inner region and $[\ \ ]_i$ the behavior near the inner bound of the outer region. Eq. (III-14) states that over the match region, the M^{th} partial sum of φ^i agrees to the N^{th} partial sum of φ^o to the order of $[\gamma(\epsilon)]$.

IV. SOLUTIONS FOR φ_o^o AND φ_o^i

As $\epsilon \to o$, the disturbance vanishes altogether, the outer flow region is just the undisturbed flow, which is independent of ϵ. These conditions will be satisfied if we take

$$f_o(\epsilon) = 1 \tag{IV-1}$$

$$f_m(\epsilon) \to o, \text{ as } \epsilon \to o \text{ for } m \geq 1 \tag{IV-2}$$

$$\varphi_o^o(x,y,s) = \int_o^s \cos\alpha(\tau)\, d\tau + x \sin\alpha(s)$$

$$= \varphi_o^o(o,o,s) + x \sin\alpha(s) \tag{IV-3}$$

where $\varphi_o^o(x,y,s)$ is the undisturbed potential in curvilinear coordinate. The matching condition, Eq. (III-14) for $m = o$, $n = o$ becoming

$$\lim_{\epsilon \to o} \frac{g_o(\epsilon)\left[\varphi_o^i\right]_o - \left[\varphi_o^o(o,o,s) + \epsilon X \sin\alpha(s)\right]}{\gamma(\epsilon)} \sim 0 \tag{IV-4}$$

It is obvious that we should take $\gamma(\epsilon) = 1$, then this gives

$$g_o(\epsilon) = 1$$

$$\left[\varphi_o^i\right]_o = \varphi_o^o(o,o,s) = \int_o^s \cos\alpha(\tau)\, d\tau \tag{IV-5}$$

Now, the inner solution stands:

$$\varphi^i \sim \varphi_o^i + g_1(\epsilon)\varphi_1^i + \ldots \tag{IV-6}$$

Substituting this equation into the basic differential equation (III-8) and basic boundary condition (III-11) gives

$$\nabla_{XY}^2 \varphi_o^i = 0 \tag{IV-7a}$$

$$\nabla_{XY}\varphi_o^i \cdot \nabla_{XY} F = \left(\frac{\partial \varphi_o^i}{\partial n}\right)_\sigma = 0 \tag{IV-7b}$$

where ∇^2_{XY} and ∇_{XY} are two-dimensional Laplacian and two-dimensional gradient operator respectively. Together with the outer boundary condition given by (IV-5a), the governing equations for φ_o^i are completely determined. The solution of this set of equations is simply:

$$\varphi_o^i = \varphi_o^o (o,o,s) \qquad \text{(IV-8)}$$

V. Solutions for φ_1^o, φ_1^i and φ_2^i

a) General solution for φ_1^o

φ_1^o has to satisfy following set of equations:

$$\nabla^2 \varphi_1^o = 0 \tag{V-1}$$

$$\lim_{x,y \to \infty} \varphi_1^o = 0 \tag{V-2}$$

With the inner boundary condition along the jet trajectory unknown. By potential theory (Ref. [19]), the most general solution satisfying these conditions can be represented as a infinite series of a line-distribution of singularities along the jet trajectory:

$$\varphi_1^o = \int_{-\infty}^{\infty} \frac{\mu_o^{(1)}(\tau)\, d\tau}{r_o} + \int_{-\infty}^{\infty} \frac{\mu_1^{(1)}(\tau) \cos\gamma(\tau)\, d\tau}{r_o^2}$$

$$+ \int_{-\infty}^{\infty} \frac{\mu_2^{(1)}(\tau)\, P_2\,[\cos\gamma(\tau)]\, d\tau}{r_o^3} + \ldots . \tag{V-3}$$

The first term is a line distribution of sources, the second term a line distribution of doublets, the third term a line distribution of quadrupoles and so on, with the symbols having following meaning:

$\mu_o^{(1)}(\tau) = \mu_o^{(1)}[\xi(\tau), \eta(\tau), \zeta(\tau)]$ Strength of source (V-4)

$\mu_1^{(1)}(\tau) = \mu_1^{(1)}[\xi(\tau), \eta(\tau), \zeta(\tau)]$ Strength of doublet

$\mu_2^{(1)}(\tau) = \mu_2^{(1)}[\xi(\tau), \eta(\tau), \zeta(\tau)]$ Strength of quadrupole

$$\bar{r}_o = \bar{i}\,(x_o - \xi) + \bar{j}\,(y_o - \eta) + \bar{k}\,(Z_o - \zeta)$$

$$r_o = |\bar{r}_o|$$

$$\cos\gamma(s) = \bar{i} \cdot \frac{\bar{r}_o}{r_o}$$

$x_o = x_1/r_t$, $y_o = y_1/r_t$, $Z_1 = Z_1/r_t$

x_o, y_o, Z_o: location of the point where the potential is to be evaluated

ξ, η, ζ: location of the singularity on the jet trajectory

P_n: nth order Largrangian polynomial

The strength $\mu_o^{(1)}$, $\mu_1^{(1)}$, $\mu_2^{(1)}$ and so on will be determined by matching with inner solutions.

In order to do the matching, the behavior of φ_1^o, near inner boundary has to be determined first. In other words, we need the asymptotic expansions (with X, Y fixed as $\epsilon \to o$) of each singularity (source, doublet, quadrupole and so on).

Fortunately, only expansions of sources and doublets are needed for our work. These expansions are obtained from Werner and Chang (Ref. [4]). In all following formula, the index i means the expansion is obtained from the i^{th} order outer solution. For example, in this section we are dealing φ_1^o, then we should take i = 1. See Fig. 3 for symbols used.

1) Asymptotic expansion of a line distribution of sources

$$\lim_{\substack{X,\ Y \text{ fixed} \\ \epsilon \to o}} \int_{-\infty}^{\infty} \frac{-\mu_o^{(i)}(\tau)\, d\tau}{r_o} \tag{V-5}$$

$$\sim (\log \epsilon)\, 2\mu_o^{(i)}(s) + \left[2\mu_o^{(i)}(s) \log (X^2+Y^2)^{\frac{1}{2}} + T_i(s)\right]$$

$$+ (\epsilon \log \epsilon)\, \mu_o^{(i)}(s)\, h(s)\, X$$

$$+ \epsilon X\left[\mu_o^{(i)}(s)\, h(s) + \mu_o^{(i)} h(s) \log (X^2+Y^2)^{\frac{1}{2}} + P_i(s)\right]$$

$$+ 0(\epsilon^2 \log \epsilon)$$

where

$$T_i(s) = \left[\int_{-\infty}^{-\delta} + \int_{\delta}^{\infty}\right] \frac{-\mu_o^{(i)}(\tau)\, d\tau}{C}$$

$$- 2\mu_o^{(i)}(s) \log 2\delta \tag{V-5a}$$

$$P_i(s) = \left[\int_{-\infty}^{-\delta} + \int_{\delta}^{\infty}\right] \frac{-\mu_o^{(i)}(\tau)\cos\beta(\tau)\,d\tau}{c^2} \qquad (V\text{-}5b)$$

$$-\mu_o^{(i)}(s)\,h(s)\log 2\delta$$

δ: a small number, which has the property: $\delta \to o$, as $\epsilon \to o$

c: the chord of the trajectory between points P and P' (Fig. 3)

β: the angle between chord c and x-direction (Fig. 3)

This expansion is correct only if $T_i(s)$ and $P_i(s)$ are independent of δ. But this can be easily proved.

2) Asymptotic expansion of a line distribution of doublets

$$\lim_{\substack{X,\,Y \text{ fixed} \\ \epsilon \to o}} \int_{-\infty}^{\infty} \frac{\mu_1^{(i)}(\tau)\cos\gamma(\tau)\,d\tau}{r_o^2} \qquad (V\text{-}6)$$

$$\sim \frac{1}{\epsilon}\,\frac{2\mu_1^{(i)}(s)\cos\theta}{(X^2+Y^2)^{\frac{1}{2}}} - (\log\epsilon)\mu_o^{(i)}(s)\,h(s)$$

$$+\left[\mu_1^{(i)}(s)\,h(s)\frac{\cos 2\theta}{2} - \mu_1^{(i)}(s)\,h(s)\log(X^2+Y^2)^{\frac{1}{2}}\right.$$

$$\left. + G_i(s)\right]$$

$$+ o(\epsilon)$$

where

$$\cos\theta = \frac{X}{(X^2+Y^2)^{\frac{1}{2}}}$$

$$G_i(s) = \left[\int_{-\infty}^{-\delta} + \int_{\delta}^{\infty}\right] \frac{\mu_1^{(i)}}{C^3}\left[-\frac{h(s)}{2}(\tau - s)^2\cos(\alpha - \alpha') + (\tau - a)\sin(\alpha - \alpha')\right]d\tau + \mu_1^{(i)}(s)h(s)\left[\log 2\delta - \tfrac{1}{2}\right]$$

(b) Governing equations for φ_1^i and φ_2^i

The inner and outer expansion stands

$$\varphi^o \sim \varphi_o^o(o,o,s) + x\sin\alpha + f_1(\epsilon)\Big[\int_{-\infty}^{\infty} \frac{-\mu_o^{(1)}(\tau)\,d\tau}{r_o} + \int_{-\infty}^{\infty} \frac{\mu_1^{(1)}(\tau)\cos\gamma\,d\tau}{r_o^2} + \int_{-\infty}^{\infty} \frac{\mu_2^{(1)} P_2(\cos\gamma)\,d\tau}{r_o^3} + \ldots\Big] + \ldots$$

with x,y finite as $\epsilon \to o$ (V-7)

$$\varphi^i \sim \varphi_o^o(o,o,s) + g_1(\epsilon)\varphi_1^i + \ldots.$$

with X,Y finite as $\epsilon \to o$ (V-8)

In matching region, we have

$$\Big[\sum_o^1 f_m(\epsilon)\varphi_m^o\Big]_i = \varphi_o^o(o,o,s) + \epsilon X\sin\alpha + f_1(\epsilon)\Big[(\log\epsilon)\,2\mu_o^{(1)} + \frac{1}{\epsilon}\,Re\Big(\frac{2\mu_1^{(1)}}{Z}\Big) + \frac{1}{\epsilon^2}\,Re\Big(\frac{2\mu_2^{(1)}}{Z^2}\Big) + \ldots.\Big] \quad (V\text{-}9)$$

$$\Big[\sum_o^1 g_m(\epsilon)\varphi_m^i\Big]_o = \varphi_o^o(o,o,s) + g_1(\epsilon)\Big[\varphi_1^i\Big]_o \quad (V\text{-}10)$$

For later convenience, we use here the complex variables Z and z:

$$Z = X + iY \quad , \quad Re(Z) = X \quad , \quad Im(Z) = Y \quad (V\text{-}11a)$$

$$z = x + iy \quad , \quad Re(z) = x \quad , \quad Im(z) = y \quad (V\text{-}11b)$$

By taking $\gamma(\epsilon) = f_1(\epsilon)$ and being simplified by the assumption $\epsilon/g_1(\epsilon) \to o$ as $\epsilon \to o$ (we will varify this assumption later), the matching condition Eq. (III-14) becomes:

$$\lim_{\varepsilon \to o} \frac{1}{f_1(\varepsilon)} \left\{ f_1(\varepsilon) \left[(\log \varepsilon)\, 2\mu_o^{(1)} + \frac{1}{\varepsilon} \operatorname{Re}\left(\frac{2\mu_1^{(1)}}{Z_1}\right) + \frac{1}{\varepsilon^2} \operatorname{Re}\left(\frac{2\mu_2^{(1)}}{Z_2}\right) + \ldots \right] \right.$$

$$\left. - g_1(\varepsilon) \left[\varphi_1^i \right]_o \right\} = 0 \qquad \text{(V-12)}$$

which gives:

$$g_1(\varepsilon) = f_1(\varepsilon) \log \varepsilon \qquad \text{(V-13)}$$

$$\left[\varphi_1^i \right]_o = 2\mu_o^{(1)}(s) \qquad \text{(V-14)}$$

$$\mu_P^{(1)} = 0, \quad \text{for } P \geq 1 \qquad \text{(V-15)}$$

Although (V-14) gives the outer boundary condition for φ_1^i, the specific form of $g_1(\varepsilon)$ is still unknown, and therefore we are unable to obtain the governing differential equation for φ_1^i. A lot of information is revealed by (V-15): it says the strength of all higher order poles are zero and the first order outer solution is a line distribution of sources only:

$$\varphi_1^o = \int_{-\infty}^{\infty} \frac{-\mu_o^{(1)}(\tau)\, d\tau}{r_o} \qquad \text{(V-16)}$$

This is just the device used by many investigators (Ref. [5,6]) to simulate the effect of entrainment. They generally used an empirical formula for the strength of the sources. In this investigation, the strength of sources, which is not yet known, will be derived as an integral part of the whole theory.

We proceed to next order. In the matching region:

$$\left[\sum_o^1 f_m(\varepsilon)\, \varphi_m^o \right] = \varphi_o^o(o,o,s) + \varepsilon X \sin\alpha + f_1(\varepsilon) \left[(\log \varepsilon)\, 2\mu_o^{(1)}(s) + \right.$$

$$\left. + 2\mu_o^{(1)}(s) \operatorname{Re}(\log Z) + T_1(s) \right] \qquad \text{(V-17)}$$

Again, using matching condition (III-14) with $\gamma(\varepsilon) = g_2(\varepsilon)$, we have

$$g_2(\epsilon) = f_1(\epsilon) = \epsilon \tag{V-18}$$

$$\left[\varphi_2^i\right]_o = X \sin\alpha + 2\mu_o^{(1)}(s)\, \mathrm{Re}\,(\log Z) + T_1(s) \tag{V-19}$$

$$g_1(\epsilon) = g_2(\epsilon) \log\epsilon = \epsilon \log\epsilon \tag{V-20}$$

Previously, it was assumed that $\epsilon/g_1(\epsilon) \to o$ as $\epsilon \to o$. Looking at (V-20), we see that this indeed is the case.

Now, the inner solution stands:

$$\varphi^i \sim \varphi_o^i + \epsilon \log\epsilon\, \varphi_1^i + \epsilon\varphi_2^i + \ldots. \tag{V-21}$$

Substituting this into the basic differential equation (III-11) gives

$$\nabla_{XY}^2 \varphi_1^i = 0 \tag{V-22}$$

$$\nabla_{XY}\varphi_1^i \cdot \nabla_{XY}F = \left(\frac{\partial \varphi_1^i}{\partial n}\right)_\sigma = 0 \tag{V-23}$$

$$\nabla_{XY}^2 \varphi_2^i = h(s)\, \frac{\partial \varphi_o^i}{\partial X} \tag{V-24}$$

$$\nabla_{XY}\varphi_2^i \cdot \nabla_{XY}F = \left(\frac{\partial \varphi_2^i}{\partial n}\right)_\sigma = 0 \tag{V-25}$$

Here, $\sigma = \sigma_j + \sigma_w$ is inner boundary, see Fig. 4.

c) Solution for φ_1^i

From Eqs. (V-22), (V-23), and (V-14), φ_1^i is governed by:

$$\nabla_{XY}^2 \varphi_1^i = 0 \tag{V-26a}$$

$$\left(\frac{\partial \varphi_1^i}{\partial n}\right)_\sigma = 0 \tag{V-26b}$$

$$\lim_{X,Y\to\infty} \varphi_1^i = 2\mu_o^{(1)}(s) \tag{V-26c}$$

The solution of this set of equations is simply:

$$\varphi_1^i(X,Y,s) = 2\mu_o^{(1)}(s) \tag{V-27}$$

Therefore, φ_1^i represents a flow field which is parallel to the jet trajectory. At each station s, the velocity of this flow field is constant throughout the whole inner region.

d) Solution for φ_2^i : The Re-entrant Flow Model

Since $\varphi_o^i = \varphi_o^o(o,o,s)$ is independent of X, Eq. (V-24) reduces to $\nabla_{XY}^2 \varphi_2^i = 0$. Together with (V-25) and (V-19), φ_2^i is governed by following set of equations:

$$\nabla_{XY}^2 \varphi_2^i = 0 \tag{V-28a}$$

$$\lim_{X,Y\to\infty} \varphi_2^i = X \sin\alpha(s) + 2\mu_o^{(1)}(s)\, \mathrm{Re}(\log Z) \tag{V-28b}$$

$$\left(\frac{\partial \varphi_2^i}{\partial n}\right)_\sigma = 0 \tag{V-28c}$$

Here, $\mu_o^{(1)}(s)$ is still unknown and will be supplied by φ_2^i.

A number of two dimensional wake models can be chosen here to give the solution of this set of equations, each will give a different inner boundary shape. The one we choose in this investigation is the "Re-entrant Flow Model" (Refs. [16,17,18]). The flow field of "Re-entrant Flow Model" is illustrated in Fig. 4. The stream line CABHF is separated from the jet at point B. B'AB is denoted by σ_j and B'H'F, BHF by σ_w. $\sigma = \sigma_j + \sigma_w$ constitutes the inner boundary. The shape of the rear surface of the jet (dotted line BFF'B') has no direct effect on the external flow since the external flow is bounded by σ_w rather than by the rear surface of the jet. The front surface of the jet (σ_j) is assumed to be a circular arc. The

geometry shape σ_w and the wake pressure Pw are characterized by cavity number Q. The actual shape of $\sigma = \sigma_j + \sigma_w$ for Q = -1.5, -2.0 and -3.0 are demonstrated in Figs. 6a, 6b and 6c, respectively.

Mathematically, the flow region of the "Re-entrant Flow Model" consists of "two sheets of Reimann surface". What we have just described is the first sheet. The re-entrant flow HH'FF' carried some fluids of the first sheet flows into the so-called second sheet. The flow field of the second sheet is shown by the dotted lines FE and F'E'. It should be noted that the second Reimann sheet is required only for mathematical consistancy of a two-dimensional wake flow problem. In context of our three dimensional theory, all fluids which flow across line $\overline{FF'}$ (Fig. 4) will be carried away by the jet to next plane further along the jet, where this fluid will cause an increase in cross-sectional area of the jet. Thus, in present formulation, entrainment is represented by the re-entrant flow.

e) $W_2(Z,s)$: The Solution of Re-entrant Flow Model

Solution to the "Re-entrant Flow Model" has been well documented (Ref. [16, 17,18]). This solution has been obtained by the method of Levi-Civita for cavity flows about curved surfaces. Only a summary is presented here. In two dimensional problem, it is convenient to work with complex variables. We are looking for the complex potential:

$$W_2(Z,s) = \varphi_2^i(Z,s) + i\Psi_2^i(Z,s) \qquad \text{(V-29)}$$

Here Ψ_2^i is the stream function. By using conformed mapping technique, both W_2-plane and Z-plane are mapped conformed onto an auxilliary plane; the ζ-plane. The shapes of the boundary $\sigma = \sigma_j + \sigma_w$ in Z-plane, w_2-plane and ζ-plane are illustrated in Fig. 5. The boundary σ in the Z-plane is transformed into a geometrically simpler shape in the ζ-plane, a semi-circle. The solution can be represented in a parameter form as:

$$\frac{1}{\sin\alpha}\frac{dw_2}{dZ}(\zeta)=\frac{1}{\sin\alpha}(U_2-iV_2)=(1-Q)^{\frac{1}{2}}\frac{(\zeta-id)(d\zeta-1)(\zeta-i)}{(\zeta+id)(d\zeta+i)(\zeta+i)}e^{F(\zeta)} \tag{V-30}$$

$$\frac{1}{R_j\sin\alpha}\frac{dw_2}{d\zeta}(\zeta)=b(1-Q)^{\frac{1}{2}}\frac{(\zeta^4-1)(\zeta^2+d^2)(d^2\zeta^2+1)}{\zeta(\zeta^2+c^2)^2(c^2\zeta^2+1)^2} \tag{V-31}$$

$$\frac{w_2}{R_j\sin\alpha}(\zeta)=-\frac{b}{2}\frac{d^2}{c^4}(1-Q)^{\frac{1}{2}}\log\left[\frac{\zeta^2}{(\zeta^2+c^2)(\zeta^2+1/c)}\right]$$

$$-b(1-Q)^{\frac{1}{2}}\frac{(c^2-d^2)(1-c^2d^2)}{2c^4}\frac{\zeta^2}{(\zeta^2+c^2)(\zeta^2+1/c^2)}+B_o \tag{V-32}$$

where

$$B_o=\frac{b}{2}(1-Q)^{\frac{1}{2}}\frac{d^2}{c^4}\log\left[\frac{c^2}{(1-c^2)^2}\right]+b(1-Q)^{\frac{1}{2}}\frac{(c^2-d^2)(1-c^2d^2)}{2c^4(1-c^2)^2} \tag{V-32a}$$

$F(\zeta)$ is Levi-Civita's Function: $F(\zeta)=iA_1\zeta-iA_3\zeta^3/3+iA_5\zeta^5/5+\ldots$

Here, the constants $A_1, A_3 \ldots$ will determine the shape of the line $\overline{AB}$ (Fig. 4). For this investigation, only two terms of $F(\zeta)$ are taken to approximate the Levi-Civita's Function,

$$F(\zeta)=iA_1\zeta-iA_3\zeta^3/3 \tag{V-33}$$

To obtain Z as a function of ζ, w_2 is eliminated between (V-31) and (V-30)

$$\frac{1}{R_j}\frac{dZ_1}{d\zeta}(\zeta)=\frac{dw_2/d\zeta}{dw_2/dZ}=b\frac{(\zeta+id)^2(d\zeta+i)^2(\zeta+i)(\zeta^2-1)}{\zeta(\zeta^2+c^2)^2(c^2\zeta^2+1)^2}e^{[-iA_1\zeta+iA_3\zeta^3/3]} \tag{V-34}$$

All together, we have b, c, d, A_1, A_3 five unknown constants. If these five constants are known eq. (V-34) can be integrated numerically by choosing a path in the ζ-plane and integrating step by step to obtain corresponding values of Z. It is desirable to extend the integration to values of Z well into the matching zone which for small values of U_∞/U_j may as much as five to ten diameters from the origin. Unfortunately, for this range of

values of Z, ζ must approach the neighborhood of the singularity c in the ζ-plane (Fig. 5), where small incremented in ζ yield unmanageably large ones in Z. To avoid this inconvenience the reverse procedure of first choosing a point in the Z-plane and determining the corresponding values of ζ by a modified Bairstow scheme (Ref. [20]) was employed.

The constants A_1, A_3, b, c, d are determined by following five conditions (Ref. 16):

1) a predetermined cavity number Q

2) a predetermined curvature at A (Fig. 5)

3) the curvature at B must be finite (Fig. 5)

4) the curvature at B must be equal to curvature at A

5) $Z(\zeta)$ must be a single valued function at $\zeta = ic$

After applying above five conditions, the following five equations result

$$\frac{(c+d)(cd+1)(c+1)}{(c-d)(cd-1)(c-1)} e^{(A_1 c + A_3 c/3)} = (1-Q)^{\frac{1}{2}} \tag{V-35a}$$

$$\frac{2}{1-c^2} + \frac{2d}{cd+1} - \frac{2d}{c(c+d)} + A_1 + A_3 c^2 = 0 \tag{V-35b}$$

$$\frac{4d}{1+d^2} + 1 + A_1 - A_3 = 0 \tag{V-35c}$$

$$\frac{(A_1 - 3A_3)(1+c^2)^4}{4(1+d^2)^2} = \frac{(A_1 + A_3)(1-c^2)^4}{8(1+d)^4} e^{(-A_1 - A_3/3)} \tag{V-35d}$$

$$b = -\frac{(A_1 + A_3)(1-c^2)^4}{8(1+h)^4} e^{(-A_1 - A_3/3)} \tag{V-35e}$$

Of course, this is another set of nonlinear equations. By suitably constructed numerical methods, this set of equations is solved to obtain the five constants for a predetermined cavity number Q. A_1 and A_3 determine the shape of σ_j. b is a scale factor. ic and id are the points in ζ-plane corresponding to

infinity and rear stagnation point in Z-plane respectively (see Fig. 5).

The procedure outlined here gives only an approximated circular arc along σ_j. The constants A_1 and A_3 are chosen so that the curvature at front stagnations point A and points of separation B and B' will have the same value. From actual numerical computation, the maximum variation of curvature between A and B is less than 2% for $Q = -2.0$. In viewing the extreme uncertainty of the shape of the jet, this is more than enough. In Fig. 6a, 6b and 6c, the actual shape of σ for $Q = -1.5$, -2.0 and -3.0.

f) Power Series Expansion of w_2 and the strength of sources μ_o^1

w_2 can be expanded into a power series having the form

$$w_2(Z,s) = \sin\alpha(s)\cdot Z + b_o(s) + a_o(s)\log Z + \sum_1^\infty \frac{a_n(s)}{Z} \qquad \text{(V-36)}$$

It should be noted that $\mathrm{Re}[w_2(Z,s) - b_o + T_1(s)]$, not $\mathrm{Re}[w_2(Z,s)]$, is the solution of the set of eqs. (V-28). From this, we obtain the behavior of φ_2^i at outer boundary of the inner region as:

$$\left[\varphi_2^i\right]_o = \left[\mathrm{Re}[w_2(Z,s) - b_o(s) + T_1(s)]\right]_o$$

$$= X\sin\alpha(s) + T_1(s) + a_o(s)\,\mathrm{Re}(\log Z) \qquad \text{(V-37)}$$

Comparing (V-37) and (V-28b) gives

$$\mu_o^{(1)}(s) = \frac{a_o(s)}{2} \qquad \text{(V-38)}$$

Thus, the strength of the line-distribution of sources for outer expansion is determined provided that $a_o(s)$ can be evaluated.

The evaluation of the constants b_o, a_o, a_1 ... in (V-36) presents some difficulty because $w_2(Z,s)$ is not an explicit function of Z. At least

three constants b_o, a_o, a_1 have to be evaluated for $\mu_o^{(1)}(s)$ and for the later matching with outer solution. The rest of this section is devoted to obtaining these three constants.

i) $a_o(s)$

Differentiating (V-36) with respect to Z gives

$$\frac{dw_2}{dZ} = \sin\alpha + \frac{a_o}{Z} - \frac{a_1}{Z^2} + \ldots . \tag{V-39}$$

By Residu theorem

$$2\pi i \frac{a_o}{R_j \sin\alpha} = \oint_{\Gamma} \frac{1}{R_j \sin\alpha} \frac{dw}{dZ} dZ = \oint_{\Gamma_1} \frac{1}{R_j \sin\alpha} \frac{dw}{d\zeta} d\zeta \tag{V-40}$$

where Γ is any circle which encloses the surface σ in Z-plane and Γ_1 is the image of Γ in ζ-plane (Fig. 5). After expanding $dw_2/d\zeta$ (V-31) into power series, (V-40) gives

$$\frac{a_o}{R_j \sin\alpha} = -\frac{b}{2}\frac{h^2}{c^4}(1-Q)^{\frac{1}{2}} \tag{V-41}$$

ii) $a_1(s)$

Multiplying (V-39) by Z and using Residu theorem again, we have

$$-2\pi i \frac{a_1}{R_j^2 \sin\alpha} = \oint_{\Gamma} \frac{1}{\sin\alpha} \frac{dw_2}{dZ} \frac{Z}{R_j} \frac{dZ}{R_j} = \oint_{\Gamma_1} \frac{1}{\sin\alpha} \frac{dw_2}{dZ} \frac{Z}{R_j} \frac{1}{R_j} \frac{dZ}{d\zeta} d\zeta \tag{V-42}$$

Next, expanding dw_2/dZ and $dZ/d\zeta$ into power series and integrate $dZ/d\zeta$ term by term:

$$\frac{1}{\sin\alpha}\frac{dw_2}{dZ}(\zeta) = b_o + b_1(\zeta - ic) + \ldots, \text{ for } |\zeta - ic| < (1-c) \tag{V-43}$$

$$\frac{1}{R_j}\frac{dZ}{d\zeta}(\zeta) = \frac{1}{(\zeta - ic)^2}\left[c_1 + c_2(\zeta - ic) + c_3(\zeta - ic)^2 + \ldots .\right]$$

$$\text{for } 0 < |\zeta - ic| < c \tag{V-44}$$

$$\frac{Z}{R_j}(\zeta) = \frac{-c_1}{\zeta - ic} + c_o + c_3(\zeta - ic) + \ldots$$

$$\text{for } 0 < |\zeta - ic| < c \tag{V-45}$$

where c_o is a constant of integration and $c_2 = o$ since Z/R_j is a single valued function of ζ. Substituting (V-43), (V-44) and (V-45) into (V-42) and simplifying it, we have

$$\frac{a_1}{R_j^2 \sin\alpha} = b_1 c_o c_1 - b_2 c_1^2 \tag{V-46}$$

where

$$c_1 = ib \frac{(c+d)^2 (cd+1)^2 (1+c)^2 (1+c^2)}{4c^3 (1-c^4)^2} e^{(A_1 c + A_3 c^3/3)} \tag{V-46a}$$

$$c_o = \lim_{\zeta \to ic} \int_i^{\zeta} \frac{1}{(\zeta - ic)^2} \left[b \frac{(\zeta + id)^2 (d\zeta + i)^2 (\zeta + i)^2 (\zeta^2 - 1)}{\zeta(\zeta + ic)^2 (c^2\zeta^2 + 1)^2} e^{(-A_1\zeta + iA_3\zeta^3/3)} - c_1 \right] d\zeta - \frac{ic_1}{(1-c)} - 1 \tag{V-46b}$$

$$b_1 = (1-Q)^{\frac{1}{2}} \left[if_1 (A_1 + A_3 c^2) + f_2 \right] e^{(A_1 c - A_3 c^3/3)} \tag{V-46c}$$

$$b_2 = (1-Q)^{\frac{1}{2}} \left\{ f_1 [2A_3 c + (A_1 + A_3 c^2)^2] + 2 i f_2 (A_1 + A_3 c^2) + f_3 \right\} e^{(-A_1 c - A_3 c^3/3)} \tag{V-46d}$$

$$f_1 = \frac{(e-d)(cd-1)(c-1)}{(c+d)(cd+1)(c+1)} \tag{V-46e}$$

$$f_2 = \frac{-2i}{(1-d)^2} \left[\frac{d(1+d^2)}{(c+d)^2} + \frac{d(1+d^2)}{(1+cd)^2} - \frac{(1+d)^2}{(1+c)^2} \right] \tag{V-46f}$$

$$f_3 = \frac{4}{(1-d)^2} \left[\frac{d(1+d^2)}{(c+d)^3} + \frac{d^2(1+d^2)}{(1+cd)^3} + \frac{(1+d)^2}{(1+c)^3} \right] \tag{V-46g}$$

The evaluation of c_o (V-46b) deserves some explanation. By suitable numerical method, (V-46b) is evaluated to give a sequence of numbers as ζ approaches ic.

This process continues until the sequence converges to a stationary value, which is just c_o. Actually, if ζ is too close to ic, the sequence will diverge eventually because of round-off error of the machine. Nevertheless, a stationary value is clearly observed before its final divergence.

iii) b_o

Examining (V-36), we can obtain b_o by the limiting process

$$\frac{b_o}{R_j \sin\alpha} = \lim_{Z\to\infty}\left[\frac{w_2}{R_j \sin\alpha}(Z) - \frac{Z}{R_j} - \frac{a_o}{R_j \sin\alpha}\log Z\right] \tag{V-47}$$

$$= \lim_{\zeta\to ic}\left[\frac{w_2}{R_j \sin\alpha}(\zeta) - \frac{Z}{R_j}(\zeta) - \frac{a_o}{R_j \sin\alpha}\left(\log\frac{Z}{R_j} + \log R_j\right)\right]$$

For $|\zeta - ic| < (1 - c)$ and $|\zeta - ic| < c$, w_2(V-32) can be expanded into a power series having the form

$$\frac{w_2}{R_j \sin\alpha}(\zeta) = \frac{d_1}{(\zeta - ic)} + d_2 \log(\zeta - ic) + d_3 + d_4(\zeta - ic) + \ldots. \tag{V-48}$$

It is easy to show that

$$d_1 = -c_1 = -b(1-Q)^{\frac{1}{2}}\frac{(c^2 - d^2)(1 - c^2 d^2)}{4c^3(1 - c^4)} \tag{V-48a}$$

$$d_2 = -\frac{a_o}{R_j \sin\alpha} \tag{V-48b}$$

$$d_3 = \frac{a_o}{R_j \sin\alpha}\log\left[\frac{ic(1 - c^2)}{2(1 + c^2)}\right] + b(1-Q)^{\frac{1}{2}}\frac{(c^2 - d^2)(1 - c^2 d^2)(3c^4 + 8c^2 + 1)}{8c^4(1 - c^4)^2} \tag{V-48c}$$

Inserting (V-48) and (V-45) into (V-47) and after some algebraic work, we arrive at:

$$\frac{b_o}{R_j \sin\alpha} = \frac{a_o}{\sin\alpha}\frac{R_{jo}}{R_j}\log\left[\frac{c(1 - c^2)^2}{2(c^2 - d^2)(1 - d^2 c^2)}\frac{1}{b(1+Q)^{\frac{1}{2}}}\frac{R_{jo}}{R_j}\right]$$

$$+ b(1 - Q)^{\frac{1}{2}}\frac{(c^2 - d^2)(1 - c^2 d^2)(3c^4 + 8c^2 + 1)}{8c^4(1 - c^4)^2} - i\pi\frac{a_o}{\sin\alpha}\frac{R_{jo}}{R_j} \tag{V-49}$$

g) Entrainment $E_2(s)$ and drag coefficient $C_{D^2}(s)$

The entrainemt $E_2(s)$, flow-rate per unit length of the jet, is assumed to be the two-dimensional flow-rate of the re-entrant flow, which is just the sink strength $-a_o$ multiplied by 2π :

$$\frac{E_2(s)}{R_j(s)\sin\alpha(s)} = \frac{-a_o}{R_j(s)\sin\alpha(s)} = \pi b \frac{d^2}{c^4}(1-Q)^{\frac{1}{2}} \tag{V-50}$$

Since b,c and d are functions of Q only, $E/R_j \sin\alpha$ is also a function of Q only.

The drag $D_2(s)$ on the jet per unit length can be easily obtained by considering momentum balance of a two-dimensional control volume which encloses the normal cross-section of the jet (Ref. [16]):

$$D_2(s) = \rho\, E_2(s)\,(\sin\alpha(s) + U_w) \tag{V-51}$$

and the drag coefficient:

$$C_{D^2} = \frac{D_2}{\frac{1}{2}\rho\, U_\infty^2\, 2R_j} = \frac{E_2(s)}{R_j(s)\sin\alpha(s)}\left(1+\frac{U_w}{\sin\alpha}\right) \tag{V-52}$$

where U_w is speed of the free streamline BHF(Fig. 4); $U_w = (1-Q)^{\frac{1}{2}}\sin\alpha$. C_{D^2} is also a function of Q only. The graph of both C_{D^2} and $E_2/R_j\sin\alpha$ are presented in Fig. 7.

VI. SOLUTIONS FOR φ_2^o, φ_3^o, φ_3^i, φ_4^i and φ_5^i

a) $\underline{\varphi_2^o \text{ and } \varphi_3^o}$

Now, the inner and outer solutions stand

$$\varphi^o = \varphi_o^o(o,o,s) + x\sin\alpha(s) + \varepsilon\int_{-\infty}^{\infty} -\frac{\frac{a_o}{2}(\tau)d\tau}{r_o} + f_2(\varepsilon)\varphi_2^o + f_3(\varepsilon)\varphi_3^o + \dots$$

with x,y finite as $\varepsilon \to o$ (VI-1)

$$\varphi^i = \varphi_o^o(o,o,s) + (\varepsilon\log\varepsilon)\,a_o(s) + \varepsilon R_e\left[Z\sin\alpha(s) + a_o\log Z + T_1(s) + \sum_1^{\infty}\frac{a_n}{Z^n}\right]$$

$$+ g_3(\varepsilon)\varphi_3^i + g_4(\varepsilon)\varphi_4^i + g_5(\varepsilon)\varphi_5^i + \dots$$

with X,Y finite as $\varepsilon \to o$ (VI-2)

As stated before, the most general solution for φ_2^o can be written as:

$$\varphi_2^o = \int_{-\infty}^{\infty} -\frac{-\mu_o^2(\tau)d\tau}{r_o} + \int_{-\infty}^{\infty}\frac{\mu_1^2(\tau)\cos\gamma(\tau)d\tau}{r_o^2} + \int_{-\infty}^{\infty}\frac{\mu_2^2(\tau)P_2(\cos\gamma)d\tau}{r_o^3}$$

$$+ \dots \qquad \text{(VI-3)}$$

After inserting (VI-3) into (VI-1) and obtaining behaviors of inner and outer solutions at matching region, we can have the matching condition (III-14) as:

$$\lim_{\varepsilon\to o}\frac{f_2(\varepsilon)\left[(\log\varepsilon)\,2\mu_o^2 + \frac{1}{\varepsilon}\mathrm{Re}\left(\frac{2\mu_1^2}{Z}\right) + \frac{1}{\varepsilon^2}\mathrm{Re}\left(\frac{2\mu_2^2}{Z^2}\right) + \dots\right] - g_2(\varepsilon)\left[\varphi_3^i\right]_o}{\gamma(\varepsilon)} = 0 \qquad \text{(VI-4)}$$

By taking $\gamma(\varepsilon) = f_2(\varepsilon)\log\varepsilon$, we have

$$g_2(\varepsilon)\log\varepsilon \qquad \text{(VI-5)}$$

$$\left[\varphi_3^i\right]_o = 2\mu_o^2(s) \qquad \text{(VI-6)}$$

$$\mu_p^2 = 0, \text{ for } P \geq 1 \qquad \text{(VI-7)}$$

Just as φ_1^o, φ_2^o is also a line distribution source only. Actually, φ_2^o is a correction to φ_1^o. In Chapter V, we obtained the local velocity at infinity in each plane normal to the jet trajectory to be sin α and this gives φ_1^o as a line distribution of sources with strength $a_o(s)/2$. We will see later that the local velocity at infinity sin α is only correct to the order of ϵ in inner region. If we go to a higher order, the local velocity at infinity has to be modified and this will, in turn, cause a correction φ_2^o to φ_1^o in outer solution.

We proceed to φ_3^o with the same technique; this time we have:

$$f_3(\epsilon) = \epsilon^2 \tag{VI-8}$$

$$\mu_2^3(s) = \frac{a_1(s)}{2} \tag{VI-9}$$

$$\mu_P^3(s) = 0 \quad , \quad \text{for } P \geq 2 \tag{VI-10}$$

(VI-9) and (VI-10) gives

$$\varphi_3^o = \int_{-\infty}^{\infty} \frac{-\mu_o^3(\tau)d\tau}{r_o} + \int_{-\infty}^{\infty} \frac{\frac{a_1}{2}(\tau)\cos\gamma(\tau)d\tau}{r_o^2} \tag{VI-11}$$

Thus, φ_3^o is a line-distribution of doublets and sources with the strength of sources μ_o^3 unknown up to know. The line distribution of doublets here is just the device used by many investigators to simulate the effect of blockage. Later, we will see that the source term represents the three-dimensional effect of curvature and growth of the cross-section of the jet.

b) The Governing Equations for φ_3^i, φ_4^i and φ_5^i

In the matching, the inner and outer solution (VI-1) and (VI-2), with the aid of (V-5) and (V-6), become:

$$\left[\sum_{0}^{3} f_m(\epsilon)\varphi_m^o\right]_i \sim \varphi_o^o(o,o,s) + \epsilon X \sin\alpha + \epsilon\Big[a_o \log\epsilon + a_o \operatorname{Re}(\log Z) + T_1$$

$$+ (\epsilon \log\epsilon)\frac{a_o}{2} h X + \epsilon X\left(\frac{a_o}{2} h + \frac{a_o}{2} h \operatorname{Re}(\log Z) + P_1\right) + 0(\epsilon^2)\Big]$$

$$+ f_2(\epsilon)\Big[(\log\epsilon)\, 2\mu_o^2 + 2\mu_o^2 \operatorname{Re}(\log Z) + T_2 + 0(\epsilon\log\epsilon)\Big]$$

$$+ \epsilon^2\Big[\frac{1}{\epsilon} a_1 \operatorname{Re}\left(\frac{1}{Z}\right) + (\log\epsilon)\left(2\mu_o^3 - \frac{a_1}{2} h\right) + \left(2\mu_o^3 - \frac{a_1}{2} h\right)\operatorname{Re}(\log Z)$$

$$+ T_3 + G_3 + \frac{a_1 h}{8}\left(\frac{\bar{Z}}{Z} + \frac{Z}{\bar{Z}}\right) + 0(\epsilon\log\epsilon)\Big] \qquad \text{(VI-12)}$$

$$\left[\sum_{0}^{5} g_m(\epsilon)\varphi_m^i\right] \sim \varphi_o^o(o,o,s) + (\epsilon\log\epsilon)\, a_o + \epsilon \operatorname{Re}\Big[\frac{Z}{\epsilon}\sin\alpha + a_o \log\frac{Z}{\epsilon} + T_1$$

$$+ \sum_{1}^{\infty} \frac{\epsilon^n a_n}{Z^n}\Big] + [f_2(\epsilon)\log\epsilon]\, 2\mu_o^2 + g_4(\epsilon)\left[\varphi_4^i\right]_o + g_5(\epsilon)\left[\varphi_5^i\right]_o \qquad \text{(VI-13)}$$

Inserting (VI-12) and (VI-13) into the matching condition (IV-14) with the assumptions $g_5(\epsilon)/\gamma(\epsilon) \to 0$, $\epsilon^2/\gamma(\epsilon) \to 0$ and $f_2(\epsilon)/\gamma(\epsilon) \sim 0(1)$ as $\epsilon \to 0$, we have:

$$\lim_{\epsilon\to o} \frac{1}{\gamma(\epsilon)}\Big\{(\epsilon^2\log\epsilon)\Big[\frac{a_o}{2} h X + \left(2\mu_o^3 - \frac{a_1}{2} h\right)\Big] + f_2(\epsilon)\Big[2\mu_o^2 \operatorname{Re}(\log Z) + T_2\Big]$$

$$- g_4(\epsilon)\left[\varphi_4^i\right]_o\Big\} = 0 \qquad \text{(VI-14)}$$

taking $\gamma(\epsilon) = \epsilon^2 \log\epsilon$, we have

$$g_4(\epsilon) = \epsilon^2 \log\epsilon \qquad \text{(VI-15)}$$

$$f_2(\epsilon) = \epsilon^2 \log\epsilon \qquad \text{(VI-16)}$$

$$g_3(\epsilon) = \log\epsilon\, f_2(\epsilon) = \epsilon^2 \log^2\epsilon \qquad \text{(VI-17)}$$

$$\left[\varphi_4^i\right]_o = \frac{a_o}{2}(s)\, h(s)\, X + \Big[2\mu_o^3 - \frac{a_1}{2}(s)\, h(s) + T_2(s)\Big]$$

$$+ 2\mu_o^2 \operatorname{Re}(\log Z) \qquad \text{(VI-18)}$$

(VI-18) gives the inner boundary condition for φ_4^i. We proceed to φ_5^i. Again, we have the matching condition for $m=3$, $n=5$ as

$$\lim_{\epsilon\to o}\frac{1}{\gamma(\epsilon)}\left\{\epsilon^2\left[\left(\frac{a_o}{2}h+P_1\right)X+\frac{a_o}{2}hX\,Re(\log Z)+\left(2\mu_o^3-\frac{a_1}{2}h\right)Re(\log Z)\right.\right.$$

$$\left.\left.+T_3+\frac{a_1 h}{8}\left(\frac{\bar{Z}}{Z}+\frac{Z}{\bar{Z}}\right)+G_3\right]-g_5(\epsilon)[\varphi_5^i]_o\right\}=0 \qquad \text{(VI-19)}$$

By taking $\gamma(\epsilon)=\epsilon^2$, this gives

$$g_5(\epsilon)=\epsilon^2 \qquad \text{(VI-20)}$$

$$[\varphi_5^i]_o=\left(\frac{a_o}{2}(s)\,h(s)+P_1(s)\right)X+T_3(s)+G_3(s)+\left[2\mu_o^3-\frac{a_1}{2}(s)\,h(s)\right]Re(\log Z)$$

$$+\frac{a_o}{2}(s)\,h(s)\,X\,Re(\log Z)+\frac{h(s)\,a_1(s)}{8}\left(\frac{\bar{Z}}{Z}+\frac{Z}{\bar{Z}}\right) \qquad \text{(VI-21)}$$

Now, the inner solution stands

$$\varphi^i\sim\varphi_o^i+(\epsilon\log\epsilon)\varphi_1^i+\epsilon\varphi_2^i+(\epsilon^2\log^2\epsilon)\varphi_3^i+(\epsilon^2\log\epsilon)\varphi_4^i+\epsilon^2\varphi_5^i$$

$$+\ldots\ldots \qquad \text{(VI-22)}$$

Substituting this back into the basic differential equation (III-8) and the basic boundary condition (III-11) give the governing differential equation as

$$\nabla_{XY}^2\,\varphi_3^i=0 \qquad \text{(VI-23)}$$

$$\nabla_{XY}^2\,\varphi_4^i=h(s)\frac{\partial\varphi_1^i}{\partial X} \qquad \text{(VI-24)}$$

$$\nabla_{XY}\varphi_5^i=h(s)\frac{\partial\varphi_2^i}{\partial X}-\left[\frac{\partial^2}{\partial s^2}-h(s)\,\frac{\partial}{\partial X}\right]\varphi_o^i \qquad \text{(VI-25)}$$

and the inner boundary condition as

$$\frac{\nabla_{XY}F}{|\nabla_{XY}F|}\cdot\nabla_{XY}\varphi_3^i=\left(\frac{\partial\varphi_3^o}{\partial n}\right)_\sigma=0 \qquad \text{(VI-26)}$$

$$\frac{\nabla_{XY}F}{|\nabla_{XY}F|}\cdot\nabla_{XY}\varphi_4^i=\left(\frac{\partial\varphi_4^o}{\partial n}\right)_\sigma=0 \qquad \text{(VI-27)}$$

$$\frac{\nabla_{XY}F}{|\nabla_{XY}F|} \cdot \nabla_{XY}\varphi_5^i = \left(\frac{\partial \varphi_5}{\partial n}\right)_\sigma = -\frac{\partial F/\partial s}{|\nabla_{XY}F|}\frac{\partial \varphi_o^i}{\partial s} \qquad \text{(VI-28)}$$

(VI-28) can be rewritten as

$$\left(\frac{\partial \varphi_5^i}{\partial n}\right)_\sigma = \frac{dn}{ds}\frac{\partial \varphi_o^i}{\partial s} \qquad \text{(VI-29)}$$

where $\bar{n}$ is the unit normal vector to σ in X-Y plane. $d\bar{n}$ represents a infinitesimile displacement in the direction of $\bar{n}$ and $\frac{dn}{ds} = \left|\frac{d\bar{n}}{ds}\right|$.

c) Solutions for φ_3^i and φ_4^i

Since φ_4^i is independent of X, (VI-24) reduces to a two-dimensional Laplace Equation. Together with (VI-27) and (VI-18), φ_4^i is governed by the following set of equations:

$$\nabla_{XY}^2 \varphi_4^i = 0 \qquad \text{(VI-30)}$$

$$\lim_{X,Y\to\infty} \varphi_4^i = \frac{a_o}{2}(s)h(s)\,X + \left[2\mu_o^3 - \frac{a_1}{2}(s)h(s) + T_2(s)\right] + 2\mu_o^2\,\mathrm{Re}(\log Z) \qquad \text{(VI-30b)}$$

$$\left(\frac{\partial \varphi_4^i}{\partial n}\right)_\sigma = 0 \qquad \text{(VI-30c)}$$

Compare this set of equations with the governing equations for φ_2^i (V-28a,b,and c), we see that the solution for φ_4^i is just the Re-entrant Flow Model with a local velocity at infinity as $a_o h_o/2$ instead of $\sin\alpha(s)$ for φ_2^i. Actually, φ_4^i is a correction to φ_2^i, i.e., the local velocity at infinity, $\sin\alpha(s)$, is only correct to $O(\varepsilon)$ and we need a correction to this if we go to a higher order $O(\varepsilon^2 \log\varepsilon)$. Of course, if the jet trajectory were straight line [$h(s) = 0$], there will be no correction whatsoever. Thus, φ_4^i represents part of three-dimensional effect of curvature on the inner solution.

Define a complex $w_4(Z,s)$ as

$$w_4(Z,s) = \frac{a_o(s)h(s)}{2\sin\alpha(s)} w_2(Z,s)$$

$$= \frac{a_o(s)h(s)}{2\sin\alpha(s)}\left[\sin\alpha Z + a_o \log Z + \sum_1^\infty \frac{a_n}{Z^n}\right] \qquad \text{(VI-35)}$$

where $w_2(Z,s)$ is the Re-entry Flow Model defined in section (V-e). Then φ_4^i and the source strength μ_o^2 for φ_2^o will be

$$\varphi_4^i(X,Y,s) = \mathrm{Re}\left[w_4(Z,s) - \frac{a_o(s)\,h(s)}{2\sin\alpha(s)}\, b_o(s) + \left[2\mu_o^3(s) - \frac{a_1}{2}(s)h(s) + T_2(s)\right]\right] \qquad \text{(VI-36)}$$

$$\mu_o^2(s) = \tfrac{1}{2}\,\frac{a_o(s)\,h(s)}{2\sin\alpha(s)}\, a_o(s) \qquad \text{(VI-37)}$$

φ_3^i is governed by (VI-23, 26, 6). The solution of this set of equations is

$$\varphi_3^i(X,Y,s) = 2\mu_o^2(s) = \frac{a_o(s)\,h(s)}{2\sin\alpha(s)}\, a_o(s) \qquad \text{(VI-38)}$$

which represents another flow field tangential to the jet trajectory.

d) $\underline{\varphi_5^i}$

The differential governing equation (VI-25) is Possion's equation with right-hand side to be a function of φ_2^i and φ_o^i. The solution of Possion's equation can be written as a sum of homogeneous solution and a particular solution

$$\varphi_5^i = \varphi_{5h}^i + \varphi_{5\,P}^i \qquad \text{(VI-39)}$$

Let $\bar{w}_2$ be the complex conjugate of w_2, then $\varphi_2^o = \tfrac{1}{2}\left[w_2(Z,s) + b_o(s) + T_1(s) + \bar{w}(\bar{Z}) + \bar{b}_o(s) + T_1(s)\right]$ and (VI-25) becomes

$$\nabla_{XY}^2 \varphi_5^i = 4\,\frac{\partial^2 \varphi_5^i}{\partial Z\,\partial \bar{Z}} = \frac{h(s)}{2}\left[\frac{dw_2}{dZ} + \frac{d\bar{w}_2}{d\bar{Z}}\right] - h(s)\sin\alpha(s) \qquad \text{(VI-40)}$$

In this form, a particular solution φ_{5P}^i is easily obtained

$$\varphi_{5P}^i(X,Y,s) = \frac{h(s)}{8}\left[\bar{Z}\,w_2(Z) + Z\,\bar{w}_2(\bar{Z}) - 2Z\bar{Z}\sin\alpha(s)\right] \qquad \text{(VI-41)}$$

With the aid of power series expansion of w_2 (V-36), we have the behavior of φ_P^5 at outer boundary of inner region as

$$\left[\varphi^i_{5P}\right]_o = \frac{h}{8}\left[\bar{Z}\, b_o + Z\,\bar{b}_o + a_o(\bar{Z}\log Z + Z\log\bar{Z}) + a_1\left(\frac{\bar{Z}}{Z}+\frac{Z}{\bar{Z}}\right)\right] \tag{VI-42}$$

The homogeneous solution should satisfy following set of equations:

$$\nabla^2_{XY}\varphi^i_{5h} = 0 \tag{VI-43a}$$

$$\left[\varphi^i_{5h}\right]_o = \left[\varphi^i_5\right]_o - \left[\varphi^i_{5P}\right]_o \tag{VI-43b}$$

$$\left(\frac{\partial\varphi^i_{5h}}{\partial n}\right)_\sigma = \frac{dn}{ds}\frac{\partial\varphi_o}{\partial s} - \left(\frac{\partial\varphi^i_{5P}}{\partial n}\right)_\sigma \tag{VI-43c}$$

Inserting (VI-21) and (VI-42) into (VI-43b) gives

$$\left[\varphi^i_{5h}\right]_o = \left(\frac{a_o}{2}h + P_1\right)X + T_3 + G_3 + \left(2\mu^3_o - \frac{a_1}{2}h\right)\mathrm{Re}(\log Z)$$
$$+ \frac{a_o h}{8}(Z\log Z + \bar{Z}\log\bar{Z}) - \frac{h}{8}\left(\bar{Z}\, b_o + Z\,\bar{b}_o\right) \tag{VI-44}$$

Attention should be called to the fact that up to now the source strength μ^3_o for φ^o_3 is still undetermined and is at our disposal. For convenience, φ^i_{5h} and μ^3_o are broken up into two parts:

$$\varphi_{5h} = \varphi_{5h1} + \varphi_{5h2} \tag{VI-44a}$$

$$2\mu^3_o - a_1 h/2 = \mu^3_{o1} + \mu^3_{o2} \tag{VI-44b}$$

where φ^i_{5h1} is governed by

$$\nabla^2_{XY}\varphi^i_{5h1} = 0 \tag{VI-45a}$$

$$\left[\varphi^i_{5h1}\right]_o = \left[\varphi^i_{5h}\right]_o - \mu^3_{o2}\,\mathrm{Re}(\log Z) \tag{VI-45b}$$

Here, the inner boundary condition for φ^i_{5h1} has not been specified. Of course, the solution to this set of equations will not be unique. By inspection, a

solution can be easily found as

$$\varphi^{i}_{5\,h1}(X,Y,s) = Re\left[\frac{a_o(s)\,h(s)/2 + P_1(s)}{\sin\alpha(s)}\left[w_2(Z,s) - b_o(s)\right]\right] + T_3(s) + G_3(s)$$

$$+ \frac{a_o(s)\,h(s)}{8}(Z\log Z + \bar{Z}\log\bar{Z}) - \frac{h(s)}{8}\left[\bar{Z}\,b_o(s) + Z\,\bar{b}_o(s)\right] \qquad \text{(VI-46)}$$

e) $\underline{\varphi^{i}_{5\,h2}}$

The governing equations for $\varphi^{i}_{5\,h2}$ are

$$\nabla^2_{XY}\varphi^{i}_{5h2} = 0 \qquad \text{(VI-47a)}$$

$$\left[\varphi^{i}_{5\,h2}\right]_o = Re\left[\mu^{3}_{o\,2}\log Z\right] \qquad \text{(VI-47b)}$$

$$\left(\frac{\partial\varphi^{i}_{5h2}}{\partial n}\right)_\sigma = \frac{dn}{ds}\frac{\partial\varphi_o}{\partial s} - \left[\frac{\partial}{\partial n}\left(\varphi^{i}_{5P} + \varphi^{i}_{5\,h1}\right)\right]_\sigma \qquad \text{(VI-47c)}$$

Let $\Psi^{i}_{5\,h2}$ be the stream function corresponding to $\varphi^{i}_{5\,h2}$, or

$$w_{5h2} = \varphi^{i}_{5h2} + i\,\Psi^{i}_{5h2} \qquad \text{(VI-48)}$$

Then we can obtain the solution for φ^{i}_{5h2} by solving a boundary value problem on Ψ^{i}_{5h2} with the more convenient inner boundary condition

$$\Psi^{i}_{5h2}(\sigma,o) = -\int_o^\sigma \frac{\partial n}{\partial s}\frac{\partial\varphi^{i}_{o}}{\partial s}\,d\sigma + \int_o^\sigma\left[\frac{\partial}{\partial n}\left(\varphi^{i}_{5P} + \varphi^{i}_{5h1}\right)\right]_\sigma d\sigma \qquad \text{(VI-49)}$$

where $d\sigma$ represents a small displacement along the boundary σ in Z-plane (Fig. 5). Due to complexity of the geometric shape of the boundary surface σ, it is very difficult to solve this boundary value problem in Z-plane. Fortunately, there are conformal mapping techniques at our disposal and the surface σ can be transformed into a geometrically simpler boundary. Through the shape in w_2-plane and ζ-plane (Fig. 5) are much simpler than the shape of σ in Z-plane, they are still somewhat complicated for our purpose. A better choice would be by the transformation

$$\eta = -\tfrac{1}{2}\left(\zeta + \frac{1}{\zeta}\right) \tag{VI-50}$$

to map the unit semi-circle in ζ-plane to the whole upper plane on η-plane (Fig. 5). In η-plane, the solution for φ^{i}_{sh2} is easily obtained

$$\Psi^{i}_{sh2}(\eta_r,\eta_i) = \frac{1}{\pi}\int_{-\infty}^{\infty} \frac{\Psi^{i}_{sh2}(\tau,o)\eta_i}{(\eta_r-\tau)^2+\eta_i^2} d\tau - \mu^3_{o2}\ \mathrm{Im}\left[\log(\eta - iC_\eta)(\eta + iC_\eta)\right] \tag{VI-51a}$$

where τ = dummy variable of integration

$\eta = \eta_r + i\eta_i$

iC_η = the position of Point C in η-plane (Fig. 5). [Point C in Z-plane is infinite.]

The harmonic conjugate function of Ψ^{i}_{sh2} is:

$$\varphi^{i}_{sh2}(\eta_r,\eta_i) = -\frac{1}{\pi}\int_{-\infty}^{\infty} \frac{\Psi^{i}_{sh2}(\tau,o)(\eta_r-\tau)}{(\eta_r-\tau)^2+\eta_i^2}\, d\tau$$

$$-\mu^3_{o2}\,\mathrm{Re}\left[\log(\eta - iC_\eta)(\eta + iC_\eta)\right] \tag{VI-51b}$$

and

$$w_{sh2}(\eta) = \varphi^{i}_{sh2} + i\Psi^{i}_{sh2} = -\frac{1}{\pi}\int_{-\infty}^{\infty} \frac{\Psi^{i}_{sh2}(\eta_r,o)}{(\eta-\tau)}\, d\tau$$

$$-\mu^3_{o2}\log(\eta - iC_\eta)(\eta + iC_\eta) \tag{VI-51c}$$

By conformal mapping technique, $w_{sh2}(\eta)$ can be transformed back into Z-plane to obtain $w_{sh2}(Z)$. However, we generally require not the potential but the velocity, i.e.:

$$\frac{dw_{sh2}}{d\eta} = -\frac{1}{\pi}\int_{-\infty}^{\infty} \frac{\frac{\partial \Psi^{i}_{sh2}}{\partial \eta_r}(\tau,o)}{(\eta-\tau)}\, d\tau - \mu^3_{o2}\left[\frac{1}{(\eta - iC_\eta)} + \frac{1}{(\eta + iC_\eta)}\right] \tag{VI-52a}$$

$$\frac{dw_{sh2}}{dZ} = \frac{dw_{sh2}}{d\eta}\,\frac{d\eta}{d\zeta} \Big/ \frac{dZ}{d\zeta} \tag{VI-52b}$$

The next step is to evaluate $\partial \Psi^{i}_{sh2}/\partial \eta_r$. Before doing this, we should clarify two more points. In section (V-d), we stated that mathematically the Re-entrant Flow Model consists of two sheets of a Riemann Surface with dotted lines EF and EF' (Fig. 5) as the boundary streamlines on the second sheet. Physically, we are only concerned with the flow field on the first sheet. All fluid flow across $\overline{FF'}$ is assumed to be carried away by the jet. But from a mathematical point of view, we have assumed that the inner boundary of our problem consists not only of the boundary lines ABHF and AB'H'F' on the first sheet but also of FE and F'E on the second sheet. More precisely, we have assumed

$$\left(\frac{\partial \varphi^{i}_{sh2}}{\partial n}\right)_{\sigma} = \frac{dn}{ds}\frac{\partial \varphi_o}{\partial s} - \left[\frac{\partial}{\partial n}\left(\varphi^{i}_{sP} + \varphi^{i}_{sh1}\right)\right]_{\sigma} \qquad \text{(VI-52c)}$$

where σ denotes the boundary ABHFE and AB'H'F'E (Fig. 5). In essence, we have introduced artificial boundary condition on EF' and EF. One natural question will be: what is the effect of this boundary condition in the second sheet on the flow field of the first sheet. In order to answer this question, another boundary condition is introduced for comparison with equ. (VI-52c), i.e.

$$\left(\frac{\partial \varphi_{sh2}}{\partial n}\right)_{\sigma} = 0 \qquad \text{on EF and EF'} \qquad \text{(VI-53)}$$

For Q=-1.5, the solutions to these two boundary conditions are calculated and found that there is essentially no difference between these two solutions, and therefore, the more convenient boundary condition (VI-53) is used in subsequent works.

Another point to be clarified is how to determine μ^{3}_{o2}. The potential $(\varphi_{sP}+\varphi_{sh1})$ will induce a flow field which is generally not tangential to the boundary σ. φ_{sh2} is introduced such that $(\varphi_{sP}+\varphi_{sh1}+\varphi_{sh2})$ will be

tangential to the boundary σ. Therefore, $\varphi_{\sigma h 2}$ along will give a net influx of fluids through the boundary σ. This flux must be supplied by "sources" at infinity in order that the equation of continuity is satisfied. But we have two infinity: one on the first sheet (C in Fig. 5) and another on the second sheet (E in Fig. 5) sources at either one of these can supply part of the flux across the boundary σ. In order to determine μ^3_{o2}, following criterion is adopted: all flux across the portion of σ on the first sheet is supplied by the infinity on the first sheet and all the flux across the portion of σ on the second sheet is supplied by the infinity E on the second sheet, i.e.

$$2\Pi\mu^3_{o2} = -\left[\Psi^i_{\sigma h 2}(F,o) - \Psi^i_{\sigma h 2}(F',o)\right] \tag{VI-53a}$$

Now, we proceed to evaluate the boundary condition in η-plane. Remembering $\partial\varphi^o_o/\partial S = \cos\alpha(s)$, we can obtain the first integral of (VI-49) as

$$-\int_o^\sigma \frac{\partial n}{\partial s}\,\frac{\partial \varphi^i_o}{\partial s}\,d\sigma = -\cos\alpha(s)\,\frac{\partial A_\sigma}{\partial s} \tag{VI-54}$$

where A_σ is the shaded area in Fig. 6a. The second integral can be evaluated in the w_2-plane. By using the analytic property of the mapping function $w_2(Z)$, it can be shown that

$$\int_o^\sigma \left[\frac{\partial}{\partial\eta}\left(\varphi^i_{\sigma P} + \varphi^i_{\sigma h 1}\right)\right]_\sigma d\sigma = \int_o^\sigma i\left(\frac{\partial}{\partial w_2} - \frac{\partial}{\partial \bar{w}_2}\right)\left(\varphi^i_{\sigma P} + \varphi^i_{\sigma h 1}\right) dw_2 \tag{VI-55}$$

Inserting $\varphi^i_{\sigma P}$ (VI-41) and $\varphi^i_{\sigma h 1}$ (VI-46), performing the differentiations and noting that $w_2 = \bar{w}_2$ on the boundary σ, we obtain

$$\Psi^i_{\sigma h 2}(\sigma,o) = -\frac{h(s)}{4}\,\mathrm{Im}\left\{\int_o^\sigma \left[a_o(\log Z + 1)\frac{dZ}{d\zeta} - Z\,\frac{d w_2}{d\zeta} + w_2\frac{dZ}{d\zeta}\right.\right.$$

$$\left.\left. - 2\bar{Z}\sin\alpha\,\frac{dZ}{d\zeta} - \bar{b}_o\frac{dZ}{d\zeta}\right]\frac{d\zeta}{d\eta}\,d\eta\right\} - \cos\alpha(s)\,\frac{\partial A_\sigma}{\partial s} \tag{VI-56}$$

where $\frac{d\zeta}{d\eta} = -1 + \frac{\eta}{\sqrt{\eta^2-1}}$.

$\frac{dw_2}{d\zeta}$ and $\frac{dZ}{d\zeta}$ are defined in (V-31) and (V-34), (VI-45) can be integrated by by numerical method in either ζ-plane or η-plane. However, it is much easier to obtain $\partial \Psi^i_{Bh2}/\partial \eta_r$ numerically since no integration is involved in this case. To obtain $\partial \Psi^i_{Bh2}/\partial \eta_r(\eta_r, o)$, we first rewrite the boundary condition (VI-49) as

$$\frac{\partial \Psi^i_{Bh2}}{\partial \sigma}(\sigma, o) = -\frac{\partial n}{\partial s}\frac{\partial \varphi_o}{\partial s} + \left[\frac{\partial}{\partial n}\left(\varphi^i_{BP} + \varphi^i_{Bh1}\right)\right]_\sigma \qquad \text{(VI-57)}$$

Again, by using analytic properties of the mapping function w_2, we can prove

$$U_\sigma \frac{d\eta}{dw_2}\frac{\partial \Psi^i_{Bh2}}{\partial \eta_r}(\eta_r, o) = U_\sigma\, i\left[\left(\frac{\partial}{\partial w_2} - \frac{\partial}{\partial \bar{w}_2}\right)\left(\varphi^i_{BP} + \varphi^i_{Bh1}\right)_\sigma - \frac{\partial n}{\partial s}\cos\alpha(s)\right] \qquad \text{(VI-58)}$$

after substituting φ^i_{BP} and φ^i_{Bh1}, this becomes (here U_σ is the velocity of Re-entrant Flow Model on σ)

$$\frac{\partial \Psi_{Bh2}}{\partial \eta_r} = -\frac{h}{4}\,\mathrm{Im}\left\{\frac{dZ}{d\eta}\left[a_o(\log Z + 1) - \bar{b}_o + \bar{w}_2 + \bar{Z}\frac{dw_2}{dZ} - 2\bar{Z}\sin\alpha(s)\right] - \frac{1}{U_\sigma}\frac{dw_2}{d\zeta}\frac{d\zeta}{d\eta}\frac{\partial n}{\partial s}\cos\alpha(s)\right. \qquad \text{(VI-59)}$$

This equation is evaluated by computer and is presented in Fig. 9 for Q = -1.5, -2.0, -3.0.

From (VI-43a), we have

$$\mu^3_{o2} = -\left[\Psi^o_{Bh2}(F, o) - \Psi^i_{Bh2}(F', o)\right]/2\pi \qquad \text{(VI-60)}$$

where Ψ^i_{Bh2} is defined by (VI-56) and points F,F' are shown in Fig. 4. If we examine (VI-56), we will see that only two terms are involved: one represents the effect of curvature h(s); another, the growth of the jet. Let

$$\mu^3_{o2} = a_{o5} + \frac{\cos\alpha(s)}{2\pi}\frac{\partial A}{\partial s} \tag{VI-61}$$

where A is the area enclosed by FAF'F (Fig. 4), and

$$a_{o5} = -\frac{1}{2\pi}\left[\Psi^i_{5h2}(F,o) - \Psi^i_{5h2}(F',o)\right] - \frac{\cos\alpha(s)}{2\pi}\frac{\partial A}{\partial s} \tag{VI-61a}$$

f) The source strength $\mu^3_o(s)$ for φ^o_3

Combining (VI-41), (VI-46), and (VI-51), we have the solution for φ^i_5 as

$$\varphi^i_5 = \frac{h}{8}\left[\bar{Z}w_2 + Z\bar{w}_2 - 2Z\bar{Z}\sin\alpha - \bar{Z}b_o - Z\bar{b}_o\right] + \frac{a_o h}{8}(Z\log Z + \bar{Z}\log\bar{Z})$$

$$+ \mathrm{Re}\left[\frac{a_o h/2 + P_1}{\sin\alpha}(w_2 - b_o) + w_{5h2}\right] + T_3 + G_3 \tag{VI-62}$$

Appropriate outer expansion of φ^i_5 is

$$\left[\varphi^i_5\right]_o = \left(\frac{a_o h}{2} + P_1\right)X + T_3 + G_3 + \left(\mu^3_{o1} + \mu^3_{o2}\right)\mathrm{Re}(\log Z)$$

$$+ \frac{a_o h}{2}X\,\mathrm{Re}(\log Z) + \frac{h a_1}{8}\left(\frac{\bar{Z}}{Z} + \frac{Z}{\bar{Z}}\right) \tag{VI-63}$$

where

$$\mu^3_{o1} = (a_o h/2 + P_1)\frac{a_o}{\sin\alpha}$$

$$\mu^3_{o2} = a_{o5} + \frac{\partial A}{\partial s}\frac{\cos\alpha}{2\pi}$$

Now, comparing (VI-63) with the outer boundary condition (VI-21) gives

$$\mu^3_o(s) = \left[\frac{a_1(s)h(s)}{4} + \frac{a^2_o(s)h(s)}{4\sin\alpha(s)} + \frac{a_{o5}(s)}{2}\right] + \frac{P_1(s)a_o(s)}{2\sin\alpha(s)} + \frac{\cos\alpha(s)}{4\pi}\frac{\partial A}{\partial s} \tag{VI-64}$$

This source reflects essentially three kinds of effect: the first term represents correction due to curvature effect; the second represents the effect of the shape of jet trajectory, i.e., the addition to the local flow induced by the singularity distributions along the rest of the jet [function P_1 is defined by (V-5b)]; the third, the growth of jet cross-section.

VII. COMPLETE POTENTIAL, VELOCITY, PRESSURE COEFFICIENT, ENTRAINMENT AND DRAG

a) φ^i, $\bar{q}^i$ and C_p^i

The results of previous sections are assembled to give the complete inner solution up to $O(\epsilon^2)$ as

$$\varphi^i(X,Y,s;\epsilon) = \int_0^s \cos\alpha(\tau)\, d\tau + (\epsilon \log\epsilon)\, a_o(s)$$

$$+ \epsilon\, \mathrm{Re}\left[w_2(Z,s) - b_o(s) + T_1(s) \right]$$

$$+ (\epsilon^2 \log^2\epsilon)\, \frac{a_o(s)\, h(s)}{2}\, \frac{a_o(s)}{\sin\alpha(s)}$$

$$+ (\epsilon^2 \log\epsilon)\, \mathrm{Re}\left\{ \frac{a_o(s)\, h(s)}{2\sin\alpha(s)} \left[w_2(Z,s) - b_o(s) \right] . \right.$$

$$\left. + \left[\frac{a_o^2(s)\, h(s)}{2\sin\alpha(s)} + a_{os}(s) + \frac{P_1(s)\, a_o(s)}{\sin\alpha(s)} \right.\right.$$

$$\left.\left. + \frac{\partial A}{\partial s}\, \frac{\cos\alpha(s)}{2\pi} + T_2(s) \right] \right\}$$

$$+ \epsilon^2 \left\{ \frac{h(s)}{8} \left[\bar{Z}\, w_2(Z,s) + Z\, \bar{w}_2(\bar{Z},s) - 2Z\bar{Z}\sin\alpha(s) \right.\right.$$

$$\left.\left. - \bar{Z}\, b_o(s) - Z\, \bar{b}_o(s) \right] \right.$$

$$+ \frac{a_o(s)\, h(s)}{8} (Z \log Z + \bar{Z} \log \bar{Z})$$

$$+ \mathrm{Re}\left[\frac{a_o(s)h(s)/2 + P_1(s)}{\sin\alpha(s)} \left[w_2(Z,s) - b_o(s) \right] + w_{sh2} \right]$$

$$\left. + T_3(s) + G_3(s) \right\} + \ldots$$

with X,Y finite as $\epsilon \to o$ (VII-1)

where w_2 and w_{5h_2} are defined in sections (V-e) and (VI-e) respectively. This complete potential for the inner solutions has not been evaluated because we generally require not the potentials but the velocities. To obtain the dimensionless velocity $\bar{q}^i$, we substitute the potentials in the following equation

$$\bar{q}^i = \nabla\left(\frac{\Phi^i}{r_t U_\infty}\right) = \nabla_{XYs}\varphi^i = \left[\frac{\bar{e}_X}{\epsilon}\frac{\partial}{\partial X} + \frac{\bar{e}_Y}{\epsilon}\frac{\partial}{\partial Y} + \frac{\bar{e}_s}{1-\epsilon h Y}\frac{\partial}{\partial s}\right]\varphi^i \qquad \text{(VII-2)}$$

After simplfication, we have

$$\begin{aligned}\bar{q}^i(X,Y,s;\epsilon) \sim\ & \bar{e}_X\left\{\left[1+(\epsilon\log\epsilon)\frac{a_o(s)h(s)}{2\sin\alpha(s)}\right]U_2 + \epsilon U_5\right\}\\ & + \bar{e}_Y\left\{\left[1+(\epsilon\log\epsilon)\frac{a_o(s)h(s)}{2\sin\alpha(s)}\right]V_2 + \epsilon V_5\right\}\\ & + \bar{e}_s\left\{\cos\alpha(s) + (\epsilon\log\epsilon)\frac{da_o}{ds}(s) + \epsilon\left[\frac{\partial\varphi_2^i}{\partial s} + h(s)X\cos\alpha(s)\right]\right\}\\ & + \ldots\\ & \text{with } X,Y \text{ finite as } \epsilon\to 0\end{aligned} \qquad \text{(VII-3)}$$

where

$U_2 - iV_2 = \frac{dw_2}{dZ}(Z,s)$, complex velocity of Re-entrant Model

$$\begin{aligned}U_5 - iV_5 = \frac{h(s)}{4}\Big\{ & a_o(s)[\log Z + 1] - \bar{b}_o(s) + \bar{w}_2(\bar{Z},s) + \bar{Z}\frac{dw_2}{dZ}(Z,s)\\ & - 2\bar{Z}\sin\alpha(s) + \frac{2a_o(s)}{\sin\alpha(s)}\frac{dw_2}{dZ}(Z,s)\Big\}\\ & + \frac{P_1(s)a_o(s)}{\sin\alpha(s)}\\ & + \frac{dw_{5h_2}}{dZ}(Z,s)\end{aligned} \qquad \text{(VII-3a)}$$

From (VII-3), it is seen that $\bar{q}^i$ consists of four elements: 1) the basic two dimensional solution dw_2/dZ; 2) corrections due to the three dimensional effect of local curvature, which is reflected by all terms containing h(s) and some part of dw_{5h}/dZ; 3) corrections due to the growth of jet cross-section, which are contained in the term dw_{5h_2}/dZ; 4) Higher order corrections due to the singularities distributed along the trajectory, which are represented by the function $P_1(s)$.

The pressure coefficient will be

$$C_p^i(X,Y,s:\epsilon) = 1 - \bar{q}^i \cdot \bar{q}^i$$

$$= \left[1 - (U_2^2 + V_2^2) - \cos^2 \alpha(s)\right]$$

$$- 2(\epsilon \log \epsilon)\left[\frac{a_o(s)h(s)}{2 \sin\alpha(s)} (U_2^2 + V_2^2) + \cos\alpha(s) \frac{da_o}{ds}(s)\right]$$

$$- 2\epsilon\left[(U_2 U_5 + V_2 V_5) + \cos\alpha(s)\left(\frac{\partial \varphi_2^i}{\partial s} + h(s) X \cos\alpha(s)\right)\right]$$

$$+ \ldots$$

with X,Y, finite as $\epsilon \to o$ (VII-4)

b) <u>φ^o and $\bar{q}^o$</u>

The complete outer solution up to $O(\epsilon^2)$ is:

$$\varphi^o(x,y,s:\epsilon) \sim \left[x \sin\alpha(s) + \int_o^s \cos(\tau)\, d\tau\right]$$

$$+ \epsilon \int_{-\infty}^{s} \frac{a_o(\tau)/2}{r_o}\, d\tau$$

$$+ (\epsilon^2 \log \epsilon) \int_{-\infty}^{\infty} \frac{a_o^2(\tau)h(\tau)/4 \sin\alpha(\tau)}{r_o}\, d\tau$$

$$+ \epsilon^2 \left[\int_{-\infty}^{\infty} \frac{-\mu_o^3(\tau)}{r_o} \, d\tau + \int_{-\infty}^{\infty} \frac{a_1(\tau)\cos\gamma(\tau)}{r_o^2} \, d\tau \right] + \ldots$$

with x,y finite as $\epsilon \to o$ (VII-5)

where

$\mu_o^3(s)$ see (VI-64)

$r_o(s)$ and $\cos\gamma$ are defined by (V-4)

The dimensionless coordinate in (VII-5) are referred to r_t. However, the more commonly used reference is R_{jo}. Therefore, the velocity $\bar{q}^o$ corresponding to φ^o is written in dimensionless system (X_o, Y_o, Z_o) referred to R_{jo}.

$$q^o \sim \bar{i} + \nabla_o \left[\int_{-\infty}^{\infty} \frac{-\mu(\tau)}{R_o} \, d\tau + \int_{-\infty}^{\infty} \frac{\frac{a_1}{2}(\tau)\cos\gamma(\tau)}{R_o} \, d\tau \right] + \ldots$$

with x,y fixed as $\epsilon \to o$ (VII-6)

where

$$\mu(S) = a_o(S)/2 + (\epsilon \log \epsilon)\, a_o^2(S)h(S)/4 \sin\alpha(S) + \mu_o^3(S)$$

μ_o^3 is defined by (VI-64)

It is seen that $\bar{q}^o$ is the superposition of three elements: 1) the basic free-stream cross-flow $U_\infty \bar{i}$; 2) a line distribution of doublets representing the local two dimensional blockage effect; 3) a line distribution of sources: the first term of the source strength reflects the effect of entrainment. The second and third term represent correction due to effect of local curvature, the growth of jet cross-section and the shape of jet trajectory as explained in section (VI-f).

c) Total Entrainment E(s)

The mass entrainment E(s) of the cross-flow at each station s is assumed to be the two dimensional flow-rate of the re-entrant flow, which can be expressed as

$$E(s) = -\int_{F}^{F'} \bar{q}^{i} \cdot \bar{n}\, d\sigma \qquad \text{(VII-7)}$$

The curve FF′ are shown in Fig. 4. Examining $\bar{q}^{i}$ defined by (VII-3) and recognizing

$$-\int_{F}^{F'} (U_2\, \bar{e}_X + V_2\, \bar{e}_Y) \cdot \bar{n}\, d\sigma = E_2(s),$$

we have

$$E(s;\epsilon) \sim E_2(s) + (\epsilon \log \epsilon) \frac{a_o(s)h(s)}{2 \sin\alpha(s)} E_2(s) + \epsilon E_5(s) + \ldots\ldots$$

$$\text{with X,Y finite as } \epsilon \to o \qquad \text{(VII-8)}$$

where

$E_2(s)$ is given by (V-50)

$$E_5(s) = -\int_{F}^{F'} (\nabla_{XY} \varphi_5^{i}) \cdot \bar{n}\, d\sigma = -\int_{F}^{F'} (\nabla_{XY} \varphi_{5p}^{i}) \cdot \bar{n}\, d\sigma + \frac{a_o(s)h(s)/2 + P_1(s)}{\sin\alpha(s)} E_2(s)$$

Since $E_2(s)/R_j(a)\sin\alpha(s)$ is a function of cavity number Q only, $E(s)/R_j(s)\sin(s)$ is a function of cavity number only up to O(1). We have assumed Q to be constant along the trajectory; therefore, E(s) will be proportional to $R_j(s)\sin\alpha(s)$ to O(1). This means that E(s) will have a maximum near the jet orifice and diminish gradually as the jet trajectory become parallel to the free cross-flow. This corresponds qualitatively at least to the physical situation.

d) Total Drag D(s)

The drag D(s) is determined by using momentum principle (Ref. [16]) applying to the system shown in Fig. 10. AB and A′B′ are two infinitely long plates symmetrically located with respect to X-axis. Since sections AA′ and BB′ are assumed to be located infinitely far away upstream and downstream, all disturbance created near the jet are subsided and the velocities q_A and q_B across these two sections are uniform.

By applying continuity equation to this system bounded by AA′BB′ and σ, we have

$$\rho E(s) = (q_A - q_B)\,\rho\,\ell \tag{VII-9}$$

and the momentum equation gives

$$(q_B^2 - q_A^2)\,\rho\,\ell - \int_F^{F'} (\rho q_X)(\bar{q}_{XY} \cdot \bar{n})\, d\sigma = (P_A - P_B)\,\ell - D \tag{VII-10}$$

where q_X is defined by the equation

$$\bar{q}^i = q_X \bar{e}_X + q_Y \bar{e}_Y + q_s \bar{e}_s$$

$$\bar{q}_{XY} = q_X \bar{e}_X + q_Y \bar{e}_Y$$

Combining (VII-9) and (VII-10), and using Bernouli's equation

$$(P_A - P_B)\,\ell = \tfrac{1}{2}\rho\,(q_B^2 - q_A^2)$$

we have

$$D = \tfrac{1}{2}\,\rho\,E\,(q_B + q_A) + \int_F^{F'} (P\,q_X)\,q_X dy \tag{VII-11}$$

Now, let $\ell \to \infty$, then $q_B \to \sin\alpha(s)$, $q_A \to \sin\alpha(s)$, we have

$$D(s) = \rho E(s) \sin\alpha(s) + \int_{F}^{F'} \rho\, q_X^2\, dy \qquad \text{(VII-12)}$$

Substituting E(s) (VII-8) and $q_X = U_2 + (\epsilon \log \epsilon)\, \frac{a_o(s)h(s)}{2 \sin\alpha}\, U_2 + \epsilon U_B$ into this expression gives:

$$D(s;\epsilon) \sim \rho \sin\alpha(s)\, E_2(s) + (\epsilon \log \epsilon)\, \frac{a_o(s)h(s)}{2 \sin\alpha(s)} \sin\alpha(s)\, \rho\, E_2(s) + \epsilon\rho \sin\alpha(s) E_B(s)$$

$$+ \int_{F}^{F'} \left[U_2^2 + 2(\epsilon \log \epsilon)\, \frac{a_o(s)h(s)}{2 \sin\alpha(s)}\, U_2^2 + 2\epsilon U_2\, U_B \right] \rho\, dy \qquad \text{(VII-13)}$$

on the curve FF′, U_2 is approximately equal to $(-U_w)$, which is a constant, and recognizing that

$$\int_{F}^{F'} U_B\, dy = -E_B(s)$$

we have

$$D(s;\epsilon) \sim \rho\, E_2(s) \left[\sin\alpha(s) + U_w \right] + (\epsilon \log \epsilon) \rho E_2(s) \frac{a_o(s)h(s)}{2 \sin\alpha(s)} \left[\sin\alpha(s) + 2\, U_w \right]$$

$$+ \epsilon\rho E_B(s) \left[\sin\alpha(s) + 2\, U_w \right] + \ldots$$

with X,Y finite as $\epsilon \to o$ (VII-14)

VIII. JET TRAJECTORY

a) Cavity Number and Trajectory

Up to now, a very important parameter remains unspecified, i.e., the cavity number Q. We have seen that the geometrical shape of inner boundary, entrainment and drag are all functions of Q. If we can derive a relationship between these three elements, then Q will be determined, and, in turn, geometrical shape, entrainment and drag will be determined accordingly. The trajectory will serve to give this relationship.

The curvature of the trajectory is directly influenced by the combined effects of pressure and shear stresses acting at the jet boundary. These stresses not only change the momentum of the original jet fluid but alter the momentum of a portion of the free stream fluid and through the agency of turbulent mixing give rise to entrainment as well. In the inviscid model employed here the role of viscous stresses has been reduced to that of accounting for the origions of the vortex sheet σ_w and the resulting wake region while turbulent mixing has been replaced by the re-entrant flow. One of the principle advantages of the model employed however is that it provides a dynamic coupling between the entainment and the pressure stresses typified by the cavity number Q. As a result, the value of Q is a determining factor in the trajectory shape, for which Margason (Ref. [10]) has provided experimental data. Thus, trajectories are computed for several values of Q and compared with Margason's trajectories.

The value of Q yielding the closest fit is then chosen for the computation of pressure coefficients.

b) Derivation of the Trajectory

In section (V-d), we assumed the front surface of the jet (σ_j, Fig. 4) to

be a circular arc with radius Rj(s), and rear surface BFF'B' unspecified. Here, we still let the shape of the rear surface remain unspecified, but the total cross-sectional area is assumed to equal an equivalent circle, e.i., $\pi R_j^2(S)$.

For an infinitesemally thin cross-sectional element (Fig. 11), the momentum equation and continuity equation can be written as

$$\frac{d\bar{M}_j}{dS} = D(S)\,\bar{e}_X + \rho E(S)\cos\alpha(s)\,\bar{e}_S \qquad \text{(VIII-1a)}$$

$$\frac{dm_j}{dS} = \rho E(S) \qquad \text{(VIII-1b)}$$

where $m_j(S)$: The rate of mass flux at station S

$$m_j = \pi R_j^2 \rho v_j \qquad \text{(VIII-2a)}$$

$\bar{M}_j(S)$: The rate of momentum flux at station S

$$\bar{M}_j = m_j v_j \bar{e}_S = \pi R_j^2 \rho v_j \bar{e}_S \qquad \text{(VIII-2b)}$$

$v_j(S)$: Velocity of the jet at station S

S: Dimensionless coordinate along trajectory $S = s_1/R_{jo}$

Here, we have taken the average velocity of the jet as $v_j(S)$(see Fig. 11). Substituting $\bar{M}_j$ and m_j into (VIII-1) and simplifying it, we arrive at:

$$\frac{d\alpha}{dS} = \frac{-D(S)}{\pi R_j^2(S)\, v_j(S)\rho} \qquad \text{(VIII-3a)}$$

$$\frac{dv_j}{dS} = \frac{E(S)}{\pi R_j^2(S)}\left[\frac{\cos\alpha(S)}{v_j(S)} - 1\right] \qquad \text{(VIII-3b)}$$

$$\frac{dR_j}{dS} = \frac{E(S)}{2\pi v_j(S) R_j(S)}\left[2 - \frac{\cos\alpha(S)}{v_j(S)}\right] \qquad \text{(VIII-3c)}$$

Now, substituting E (VII-8) and D (VII-14) and after some algebraic work, we finally have

$$\frac{d\alpha}{dS} = -\frac{E_o \sin^2\alpha(S)}{\pi R_j(S) v_j^2(S)} \left[(1+U_o) + (\epsilon \log \epsilon) \frac{a_o h}{2\sin\alpha} (1+2U_o) + \epsilon \frac{E_5}{E_2}(1+2U_o) \right] \quad \text{(VIII-4a)}$$

$$\frac{dv_j}{dS} = \frac{E_o \sin\alpha(S)}{\pi R_j(S)} \left(\frac{\cos\alpha(S)}{v_j} - 1 \right) \left[1 + (\epsilon \log \epsilon) \frac{a_o h}{2\sin\alpha} + \epsilon \frac{E_5}{E_2} \right] \quad \text{(VIII-4b)}$$

$$\frac{dR_j}{dS} = \frac{E_o \sin(S)}{2\pi v_j(S)} \left(2 - \frac{\cos\alpha(S)}{v_j(S)} \right) \left[1 + (\epsilon \log \epsilon) \frac{a_o h}{2\sin\alpha} + \epsilon \frac{E_5}{E_2} \right] \quad \text{(VIII-4c)}$$

with the initial conditions

$$\alpha(o) = \pi/2 \quad \text{(VIII-4d)}$$

$$v_j(o) = U_j \quad \text{(VIII-4e)}$$

$$R_j(o) = 1 \quad \text{(VIII-4f)}$$

where

$$E_o = \frac{E_2}{R_j \sin\alpha} = \pi b \frac{d^2}{c^4} (1-Q)^{\frac{1}{2}}$$

a function of Q only, see (V-50)

$$U_o = \frac{U_w}{\sin\alpha} = (1-Q)^{\frac{1}{2}}$$

also a function of Q only.

This is a set of coupled nonlinear first order differential equations. We cannot integrate them immediately, because we do not know ϵ beforehand. But we can solve it by iteration methods. First, take only terms up to O(1) i.e., the first term in the brackets, integrate them by suitable numerical

methods to get $\alpha(S)$, $R_j(S)$ and $v_j(S)$. Then we obtain the actual trajectory by integrating numerically the following set of differential equations

$$\frac{dX_o}{dS} = \cos\alpha(S) \qquad \text{(VIII-5a)}$$

$$\frac{dZ_o}{dS} = \sin\alpha(S) \qquad \text{(VIII-5b)}$$

with the initial conditions

$$X_o(o) = 0 \qquad \text{(VIII-5c)}$$

$$Z_o(o) = 0 \qquad \text{(VIII-5d)}$$

where X_o, Z_o are dimensionless Cartesian coordinates, see Fig. 11.

From the solution of this set, ϵ, $h(S)$, $P_1(S)$ are obtained and substituted back into (VIII-4). Now, we can take the full equations and integrate them again. This process is continued until the difference between two successive solutions are small. For the value of U_∞/U_j considered here, the vary first integration was accurate enough for our purpose. In Fig. 12, trajectory for U_∞/U_j = .8, .5 and .25 are plotted with Margason's curve. The jet velocity $v_j(S)$ and jet radius $R_j(S)$ along the trajectory are shown in Fig. 13 and Fig. 14, respectively.

IX. CONCLUSIONS

The inner and outer solution for pressure coefficient for $U_\infty/U_j = .8$, .5 and .25 are presented in Fig. 18, Fig. 19 and Fig. 20, respectively. Experiment data by Bradbury and Wood (Ref. [7]) and by Vogler (Ref. [8]) are also presented with the outer solutions for comparison.

Since the reentrant flow model introduces a stagnation point behind the jet, it is incapable of reproducing the experimental pressure contours in the wake region. However, upstream of and along the sides of the jet, the computed pressure contour gives good agreement with the experimental data for $U_\infty/U_j = .25$. For $U_\infty/U_j = .5$ and .8, the computed pressure contour seems to have the right order of magnitude but is not swept back enough. It is possible that the inclusion of higher order terms would remedy this as indicated by the comparison of first order and second order solutions in Ref. [4].

As indicated in the introduction, Werner and Chang (Ref. [4]) raised the possibility that representing the effects of entrainment by a net sink distribution along the jet trajectory might not be correct. In order to answer this question, we have calculated the contributions to the source strength from the various elements of the flow. In our solution, the outer flow region is represented by a line distribution of doublets and sources. The doublets simulate the effect of "local blockage", while the sources, as we have repeatedly stated, are derived from four different origins: 1) the entrainment, 2) the growth of the jet cross-sectional area, 3) the curvature effect, and 4) higher order correction due to singularities distributed along the jet trajectory, i.e., the effect of $P_1(s)$ (V-5b). The magnitude of these contributions as a function of s_1/R_{jo} are shown in Fig. 15, Fig. 16 and Fig. 17 for $U_\infty/U_j = .8$, .5 and .25, respectively. From these results, the following conclusions are drawn:

1) The source strength due to $P_1(s)$ has been calculated and proved to be very small for all cases. Actually, it is too small to be shown on these graphs.

2) Around $U_j/U_\infty = .8$, the combined effect of entrainment and jet growth is small. In other words, if only the source due to curvature is used, a good approximation is obtained.

3) At $U_\infty/U_j = .25$, the effect of curvature is much smaller than the combined effect of entrainment and growth of the jet.

Judging from the trend, we can neglect curvature effect for $U_\infty/U_j \leq .125$.

4) Introducing

$$\left(\frac{s_1}{R_{jo}}\right)_o = 4.5\left(\frac{U_j}{U_\infty}\right) - 3 \qquad \text{(IX-1)}$$

we see that the source strength due to entrainment and the source strength due to growth of the jet tend to cancel each other for

$$s_1/R_{jo} > (s_1/R_{jo})_o$$

5) It seems that, for $s_1/R_{jo} < (s_1/R_{jo})_o$, following two equations will give a reasonable approximation

$$\mu_e = C_1 \quad , \quad \text{for } \frac{s_1}{R_{jo}} \leq 4.5\left(\frac{U_j}{U_\infty}\right) - 3 \qquad \text{(IX-2)}$$

$$\mu_g = C_2 \frac{s_1}{R_{jo}}, \quad \text{for } \frac{s_1}{R_{jo}} \leq 4.5\left(\frac{U_j}{U_\infty}\right) - 3 \qquad \text{(IX-3)}$$

where C_1, C_2 are constants

μ_e: source strength due to entrainment

μ_g: source strength due to growth of the jet

X. REFERENCES

[1] Fricke, S.B., Wooler, P.T., and Ziegler, H., "A wind tunnel investigation of jets exhausting into a cross-flow", Technical Report AFFDL-TR-70-154.

[2] Mosher, David K., "An experimental investigation of a turbulent jet in a cross-flow", Ph.D. Thesis, School of Aerospace Engineering, Georgia Institute of Technology, December 1970.

[3] Keffer, J.T., Baines, W.D., "The round turbulent jet in a cross-wind", Journal Fluid Mechanics, Vol. 15, Pt. 4, April 1963, pp. 481-497.

[4] Werner, J., Chang, H., "Analytical determination of the induced flow due to a jet in a subsonic cross-flow", NYU Report AA-70-21, School of Engineering and Science, New York University, New York, New York, September 1970.

[5] Wooler, P.T., Burghart, G.H., and Gallagher, J.T., "Pressure distribution on a rectangular wing with a jet exhausting normally into an airstream", J. Aircraft, Vol. 4, No. 6, Nov.-Dec. 1967, pp. 537-543.

[6] Symposium: "Analysis of jet in a subsonic crosswind", NASA SP-218, September 9-10, 1969.

[7] Bradbury, L.J.S., Wood, M.M., "The static pressure distribution around a circular jet exhausting normally from a plane wall into airstream", C.P. No. 822, Brit. A.R.C., 1965.

[8] Jordinson, R., "Flow in a jet directed normal to the wind", R.&M. No. 3074, British A.R.C., 1958.

[9] Vogler, R.D., "Surface pressure distribution induced on a flat plate by a cold air jet issuing perpendicularly from the plate and normal to a low speed free stream flow", NASA TN D-1629, 1963.

[10] Marguson, R.J., "The path of a jet directed at large angles to a subsonic free stream", TN D-4919, November 1968.

[11] Rubbert, P.E., Saaris, G.R., "A general three-dimensional potential flow method applied to V/STOL aerodynamics (preprinted) 680304, Soc. Automat. Eng., April-May 1968.

[12] Abramovich, G.N., "The theory of turbulent jets", MIT Press, C. 1963.

[13] Cole, J.D., "Perturbation methods in applied mathematics", Ginn Blaisdell, 1968.

[14] Kaplan, S., "Fluid mechanics and singular perturbations", Academic Press, 1967.

[15] Van Dyke, M., "Perturbation methods in fluid mechanics", Academic Press, 1964.

[16] Gurevich, M.I., "Theory of jets in ideal fluids", Academic Press, 1965.

[17] Birkhoff, G., Zarantorrollo, E.H., "Jet wake and cavities", Academic Press, 1957.

[18] Milne-Thompson, L.M., "Theoretical hydrodynamics", fifth edition, The MacMillian Co., 1968.

[19] Kellogg, O.D., "Foundation of potential theory", Dover Publication, New York, 1953.

[20] Henrici, P., "Elements of numerical analysis", John Wiley & Sons, 1964.

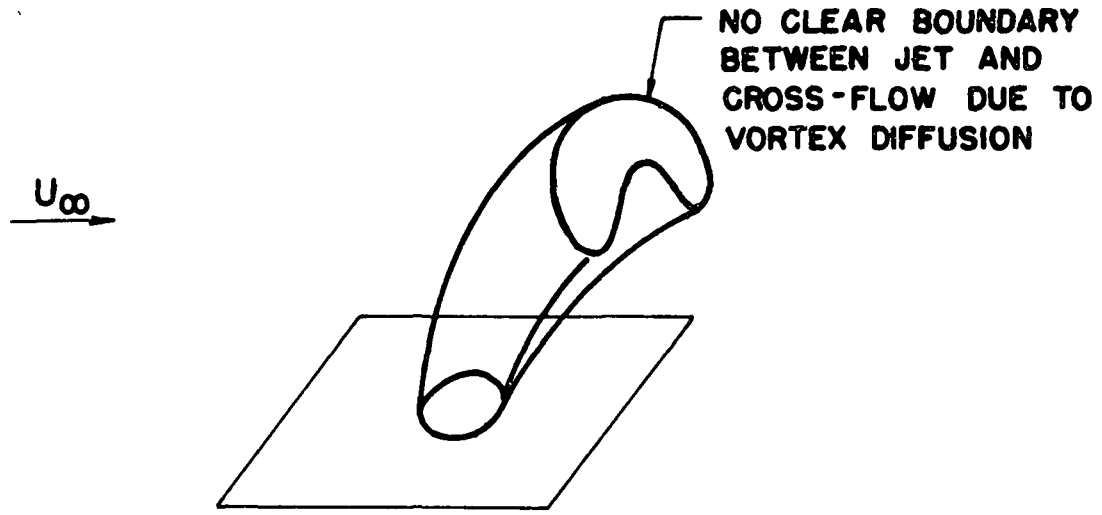

REAL JET

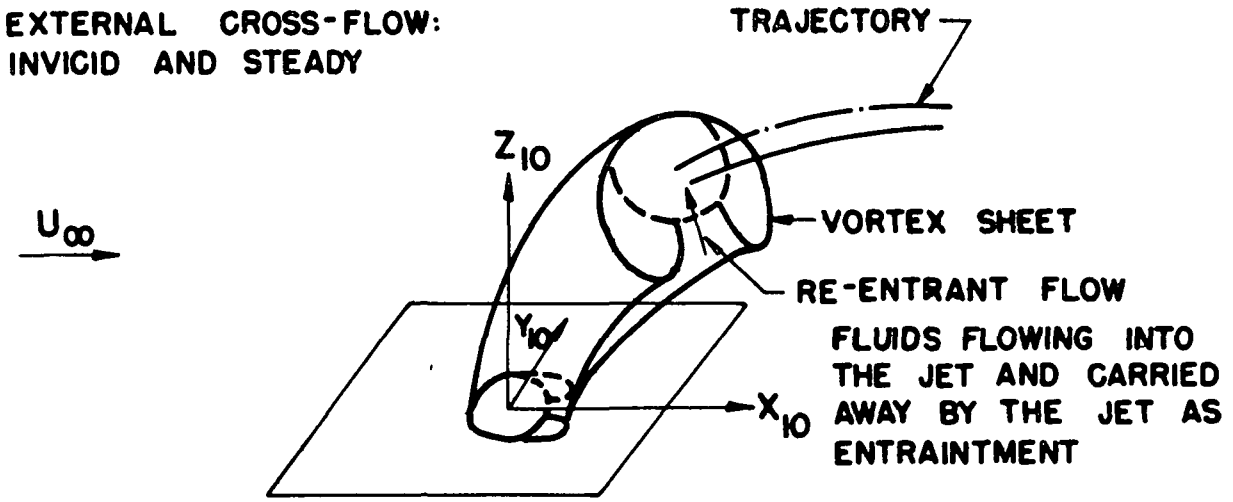

MATHEMATICAL MODEL

Fig. 1 - Jet In A Cross-flow And Mathematical Model

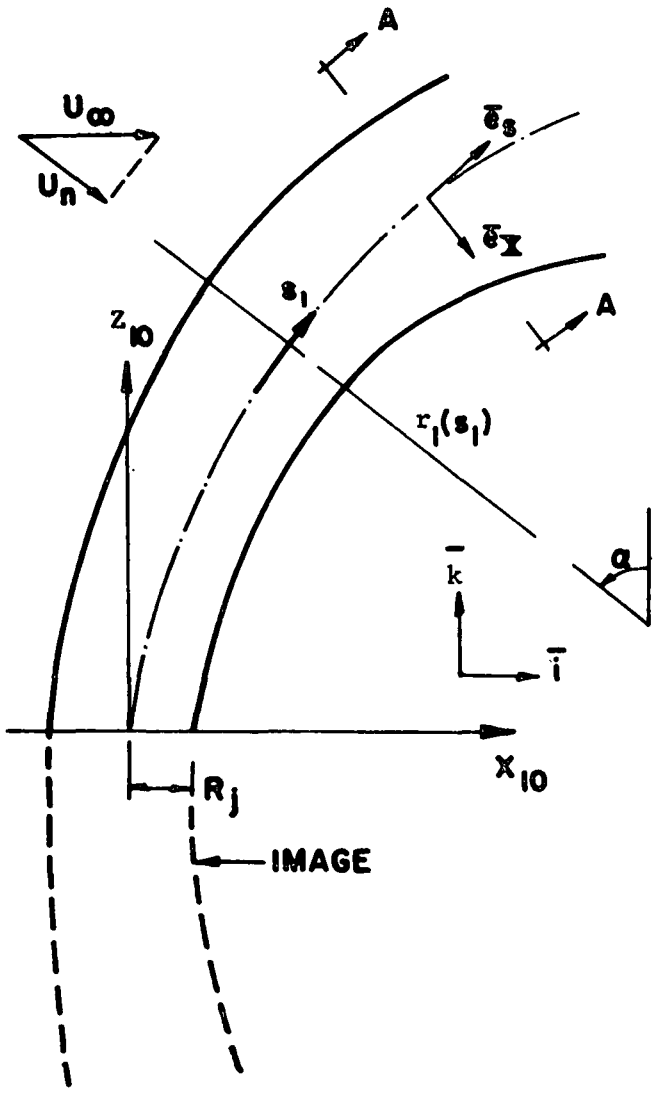

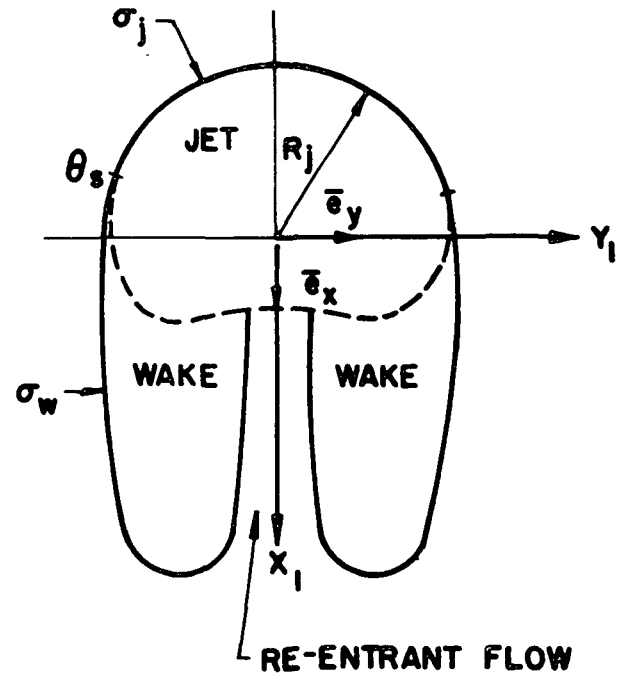

SECTION A-A

Fig. 2 - Coordinate System

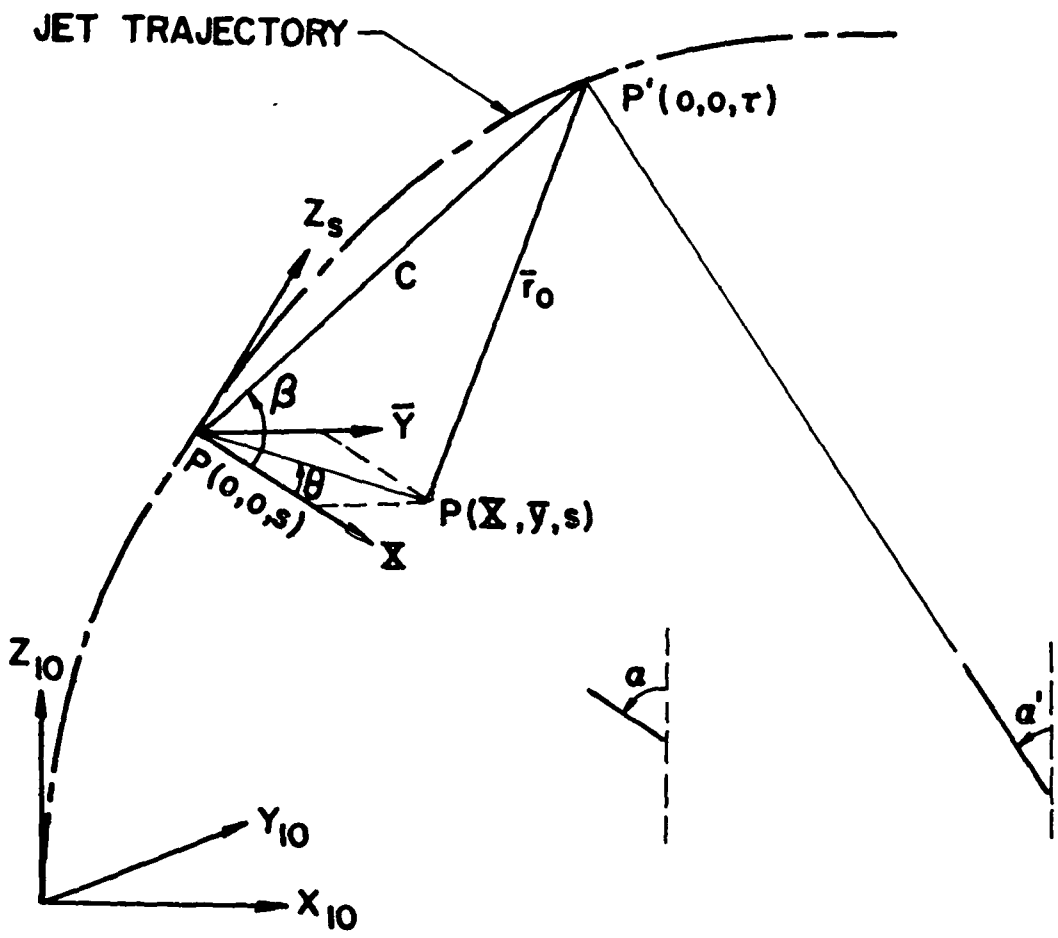

Fig. 3 - Local Coordinate System

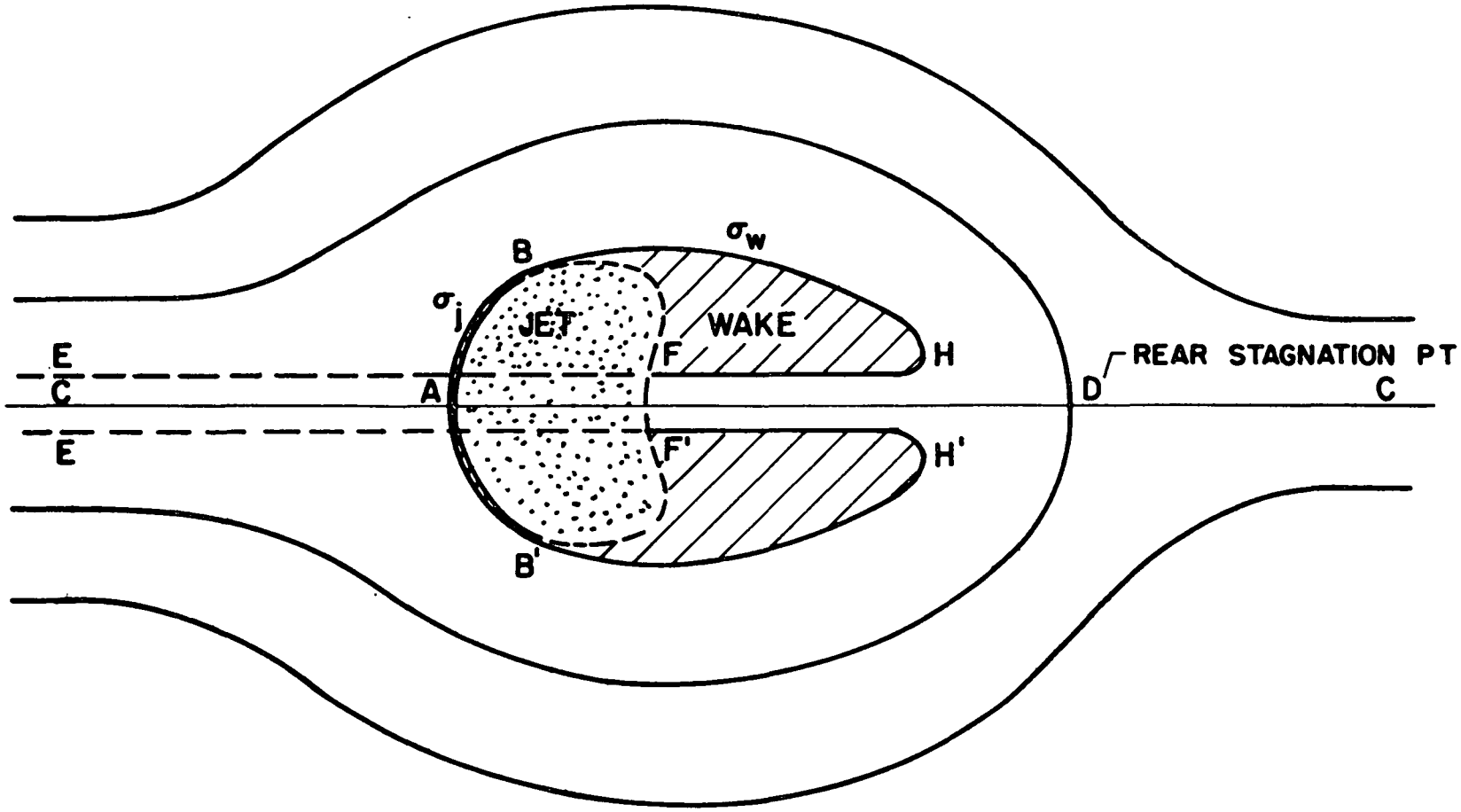

Fig. 4 - Re-entrant Flow Model

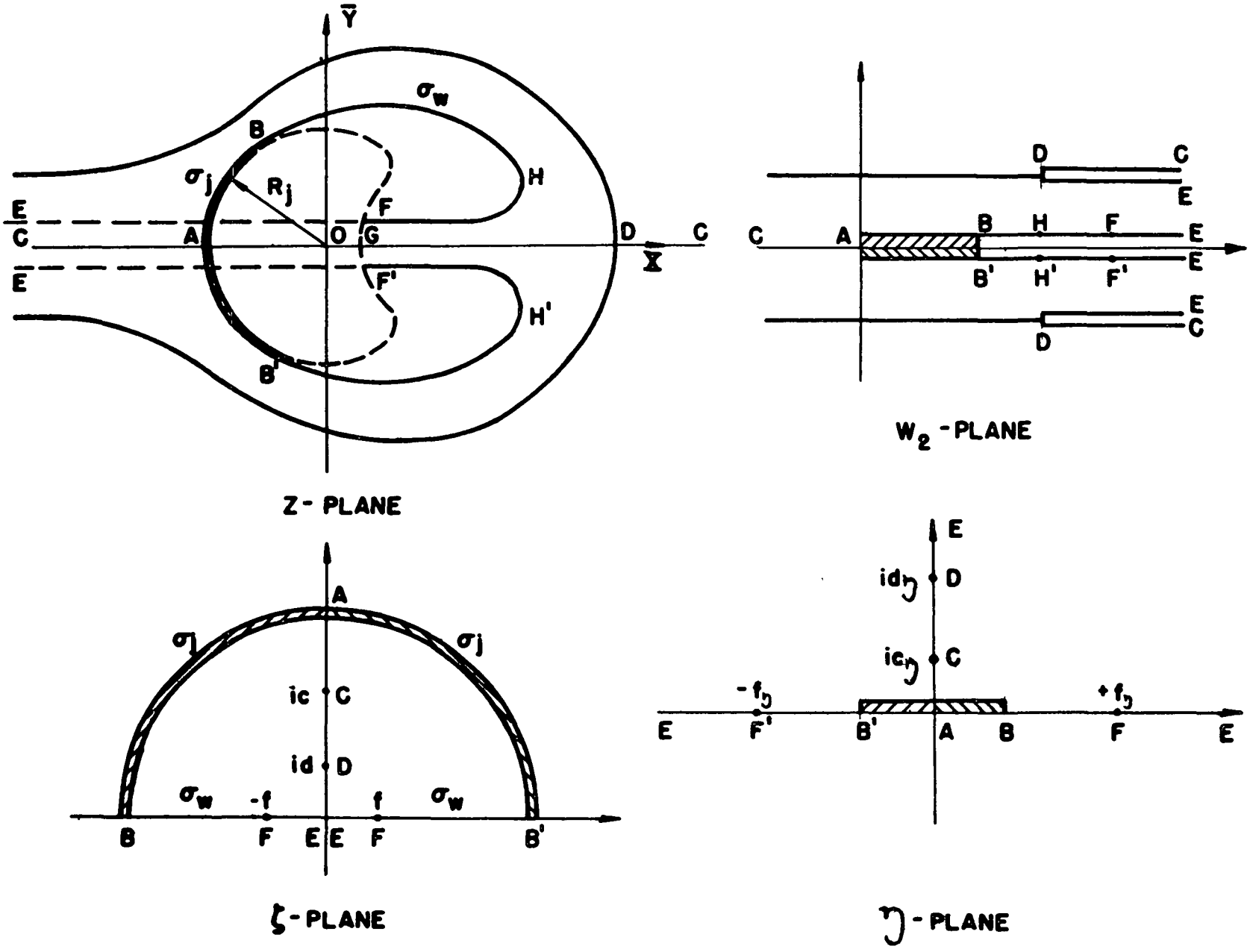

Fig. 5 - Z, w, ζ and η Mapping Planes

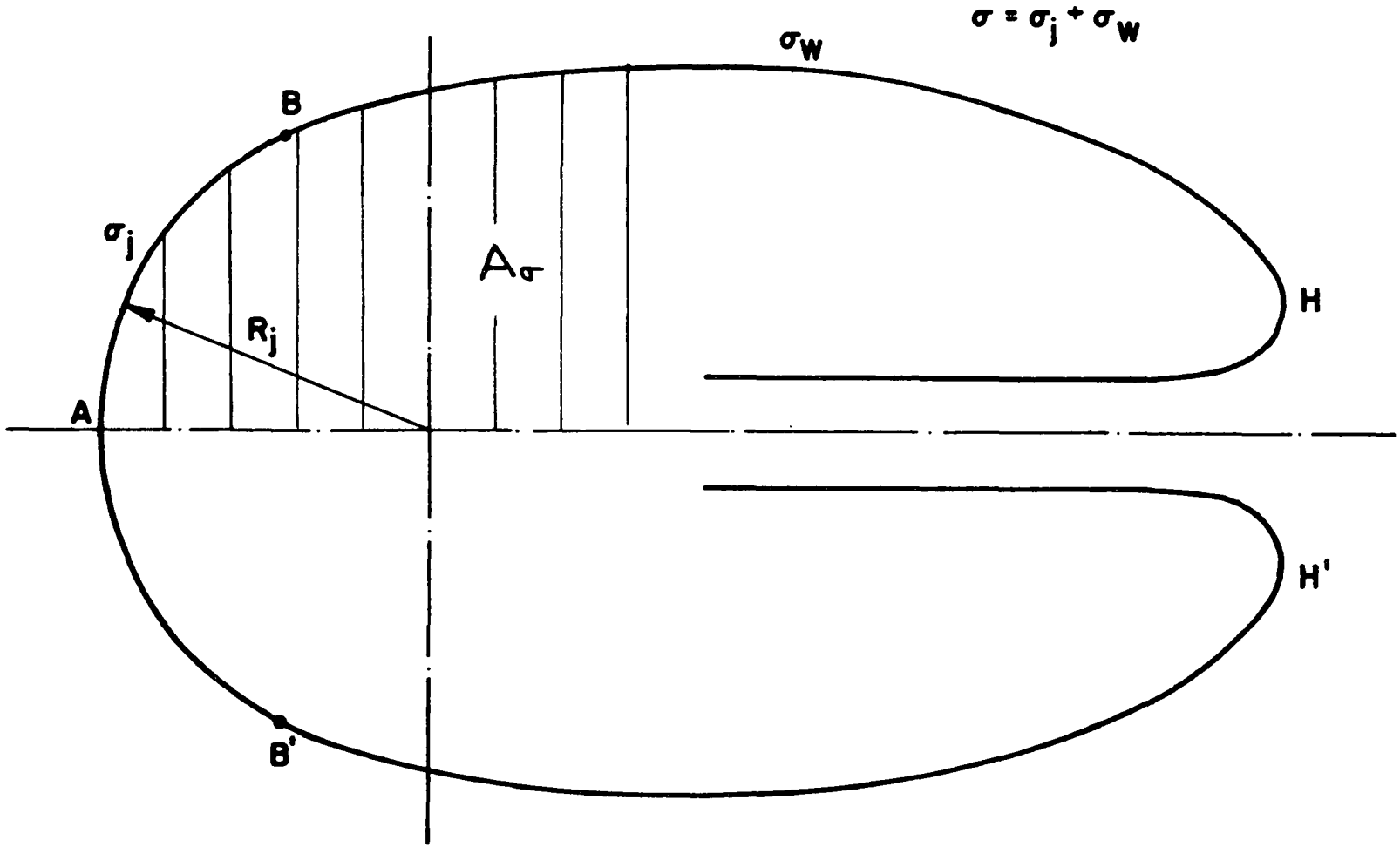

Fig. 6a - Contour σ, Q =-1.5

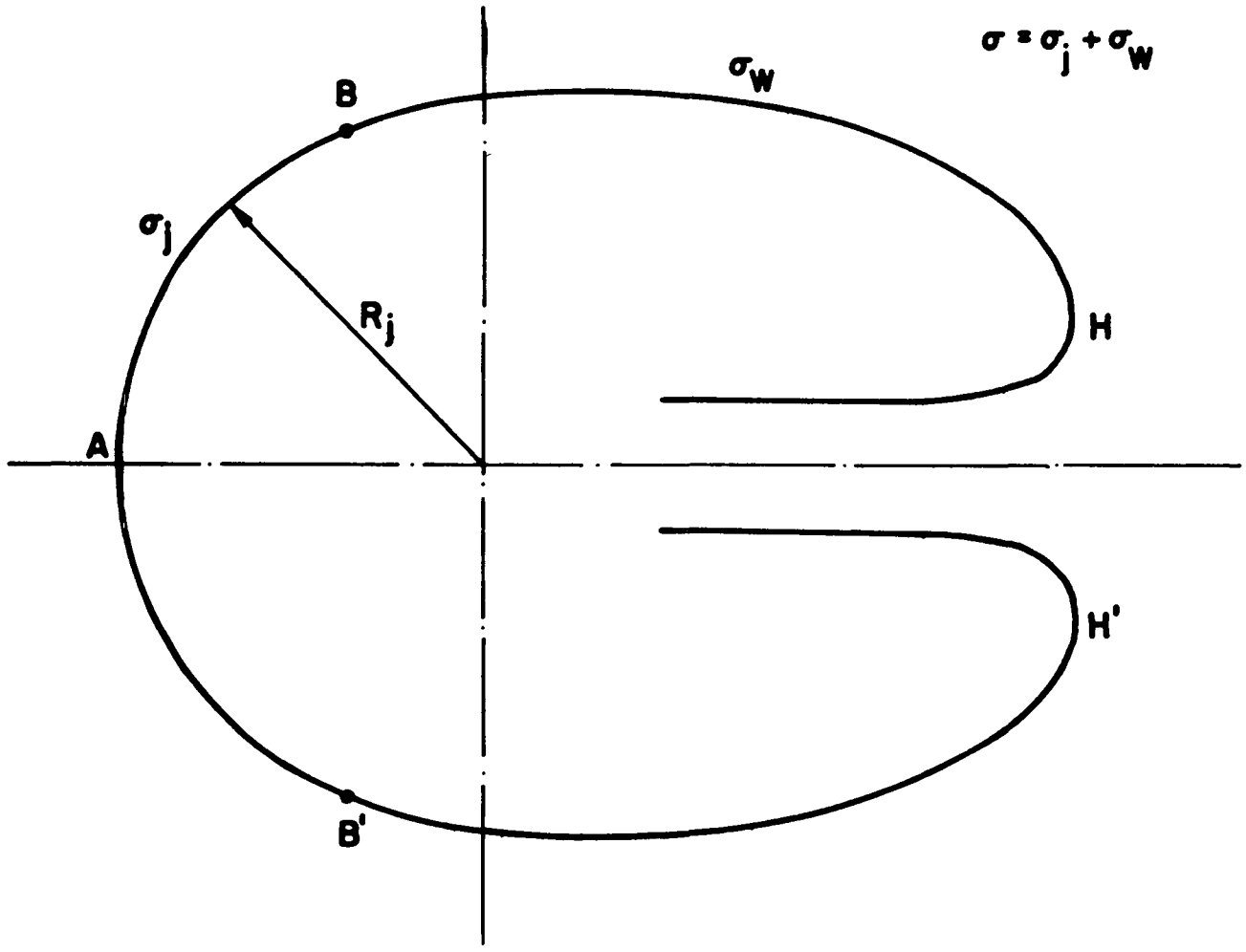

Fig. 6b - Contour σ, Q = -2.0

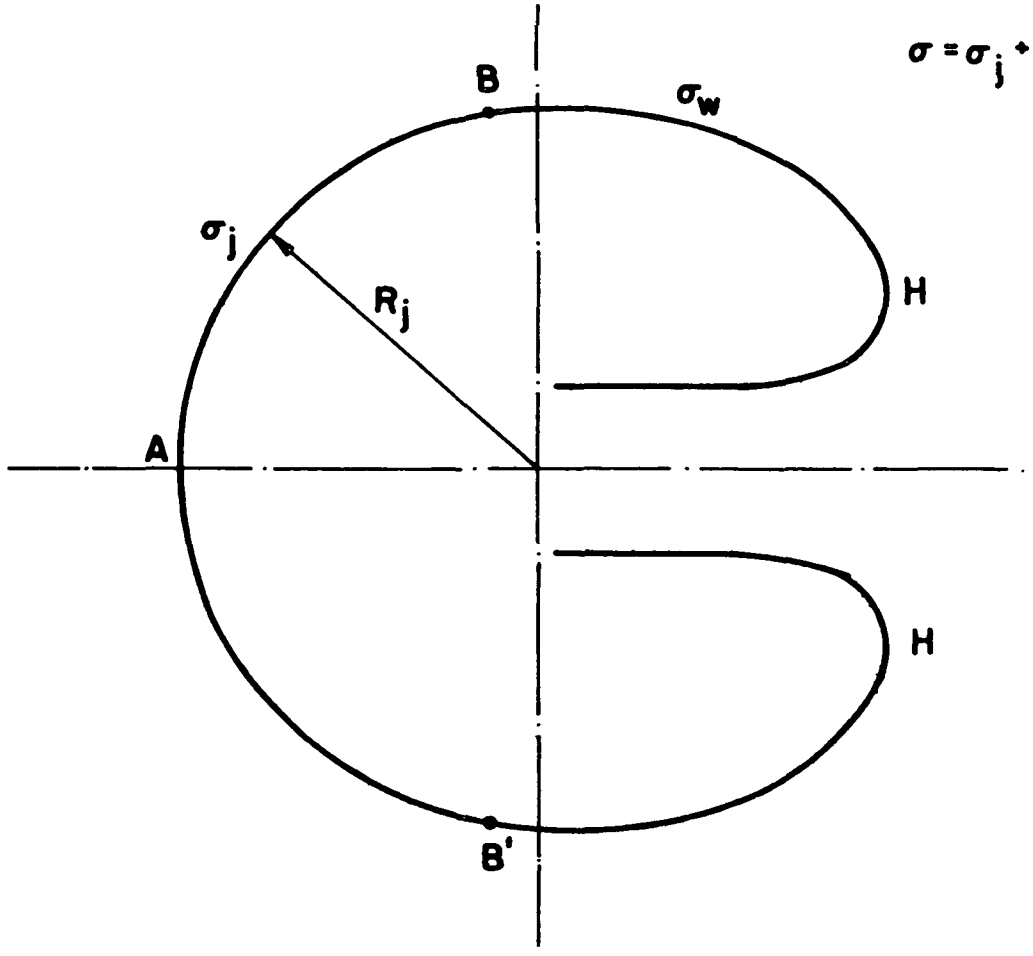

Fig. 6c - Contour σ, Q = -3.0

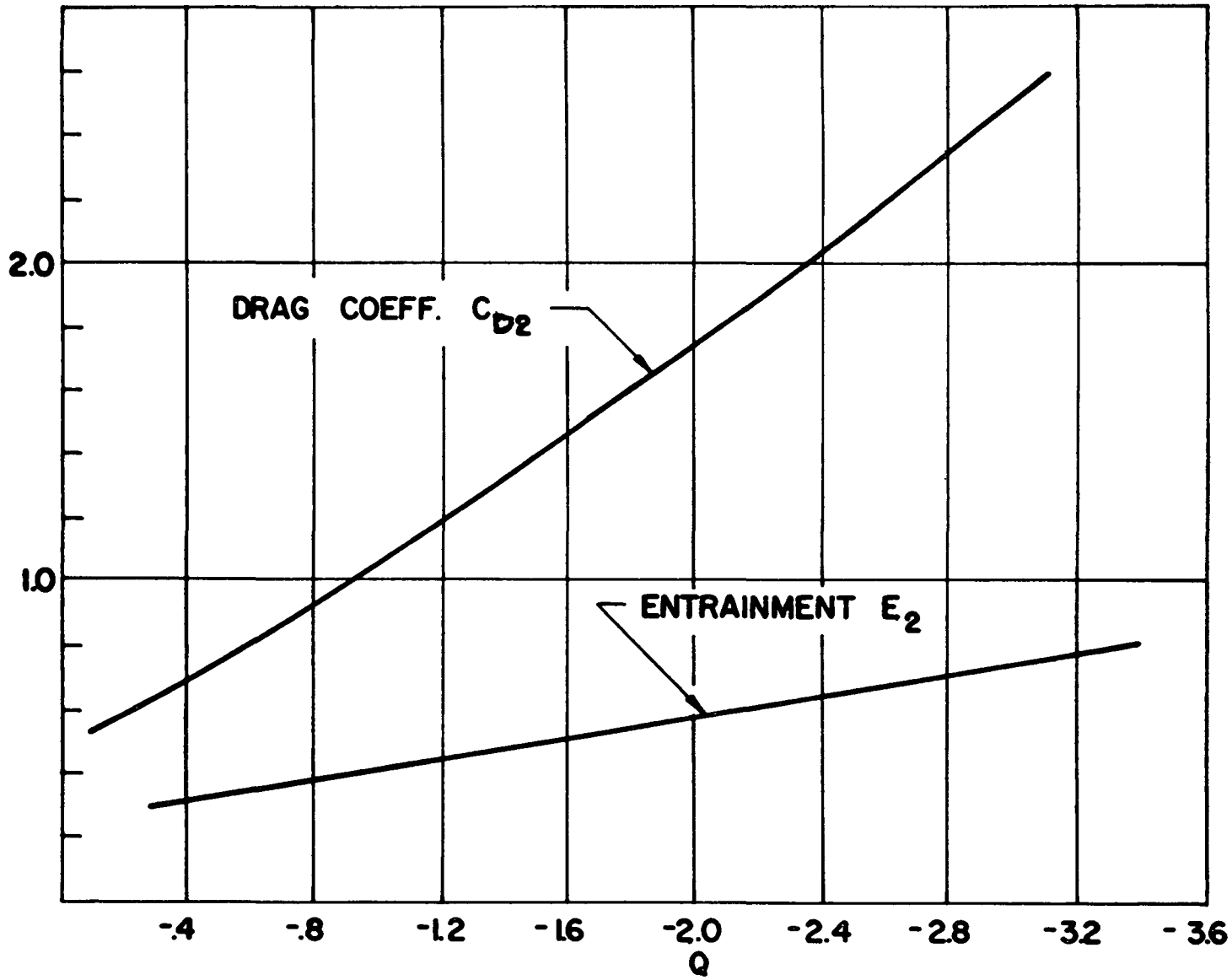

Fig. 7 - Entrainment E_2 and Drag Coefficient C_{D2} vs. Q, Re-entrant Flow Model

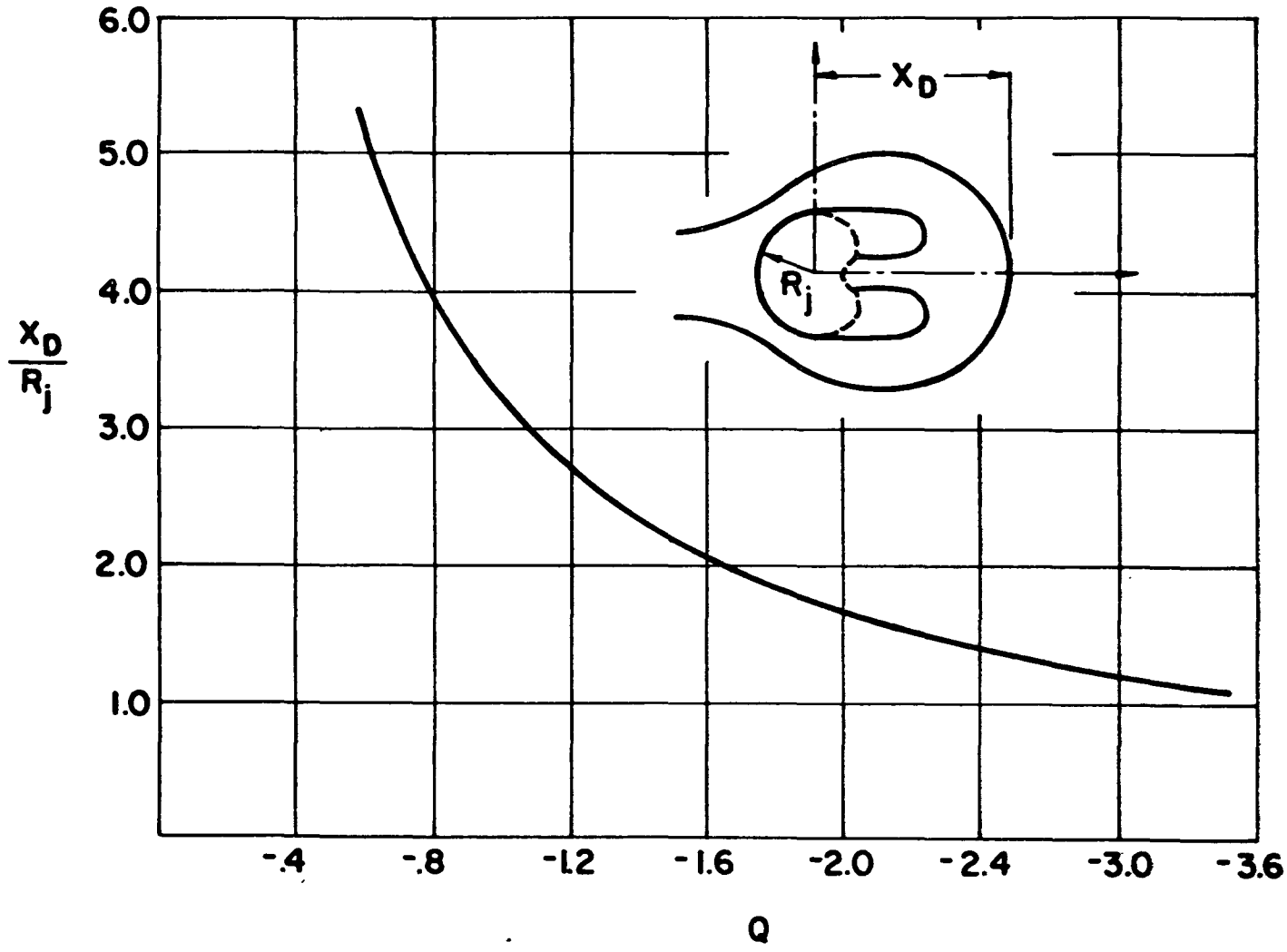

Fig. 8 - Position Of Rear Stagnation Point vs. Q, Re-entrant Flow Model

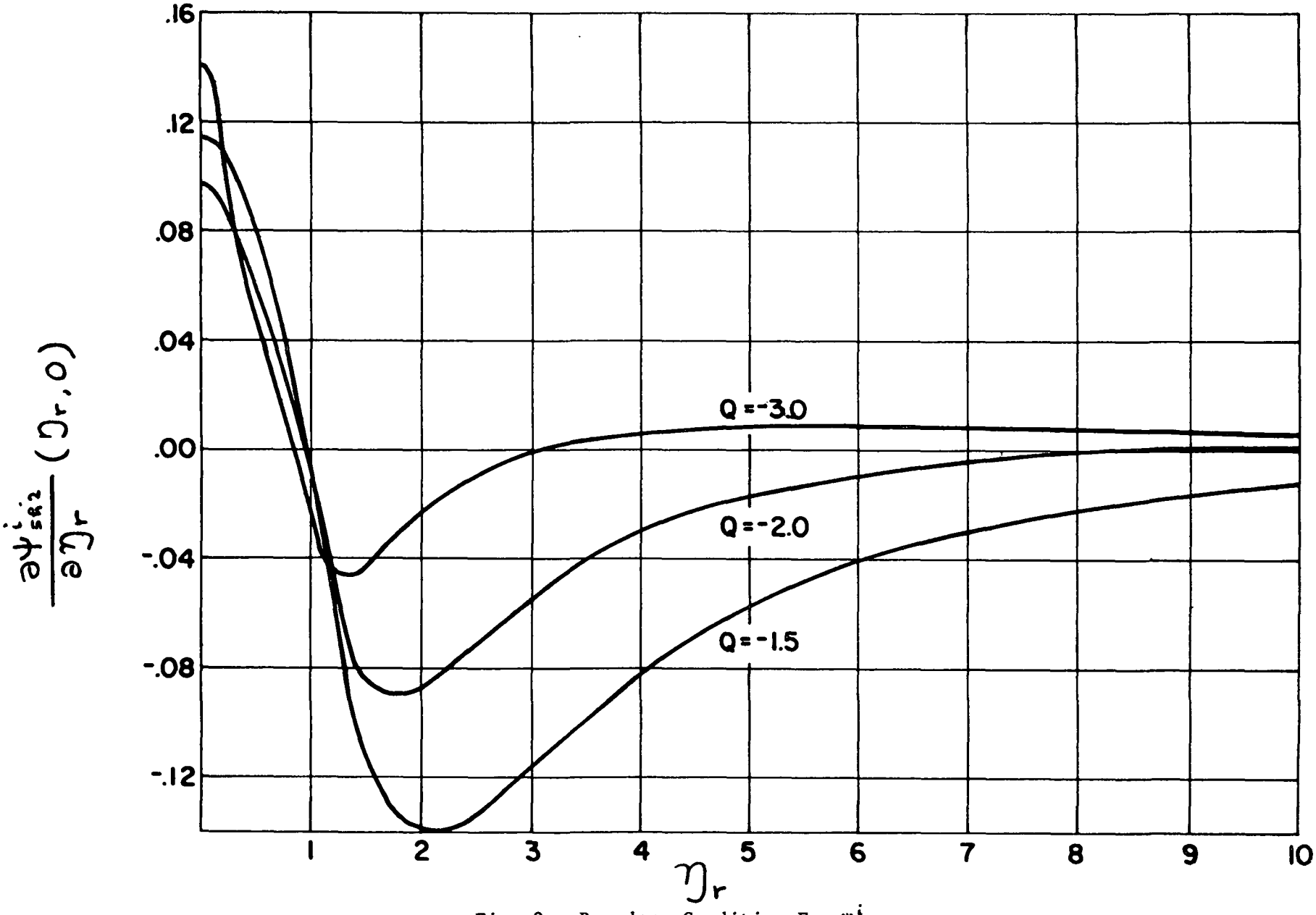

Fig. 9 - Boundary Condition For ψ^i_{sh2}

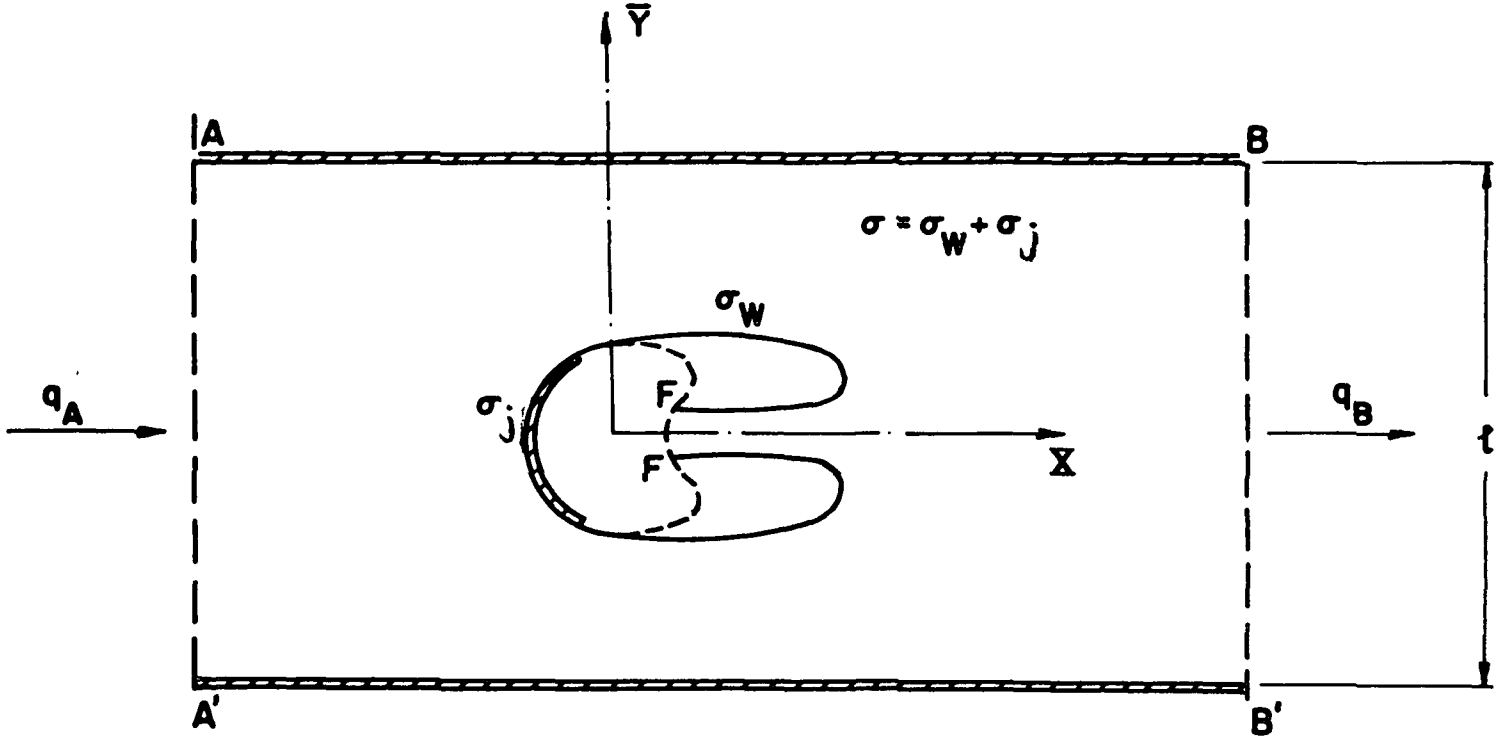

Fig. 10 - Control Volume For Determination Of Drag D(s)

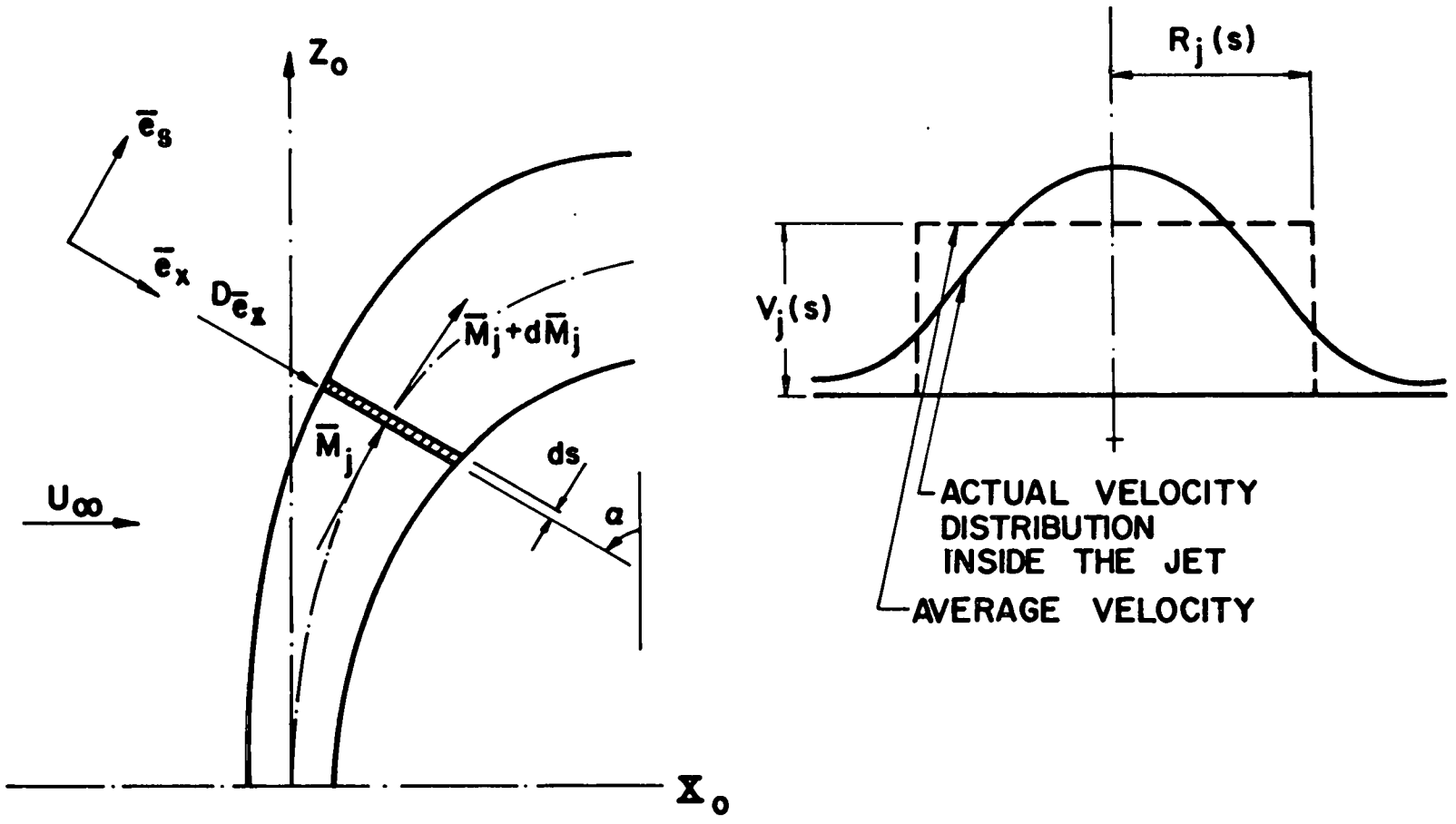

Fig. 11 - Derivation Of Jet Trajectory

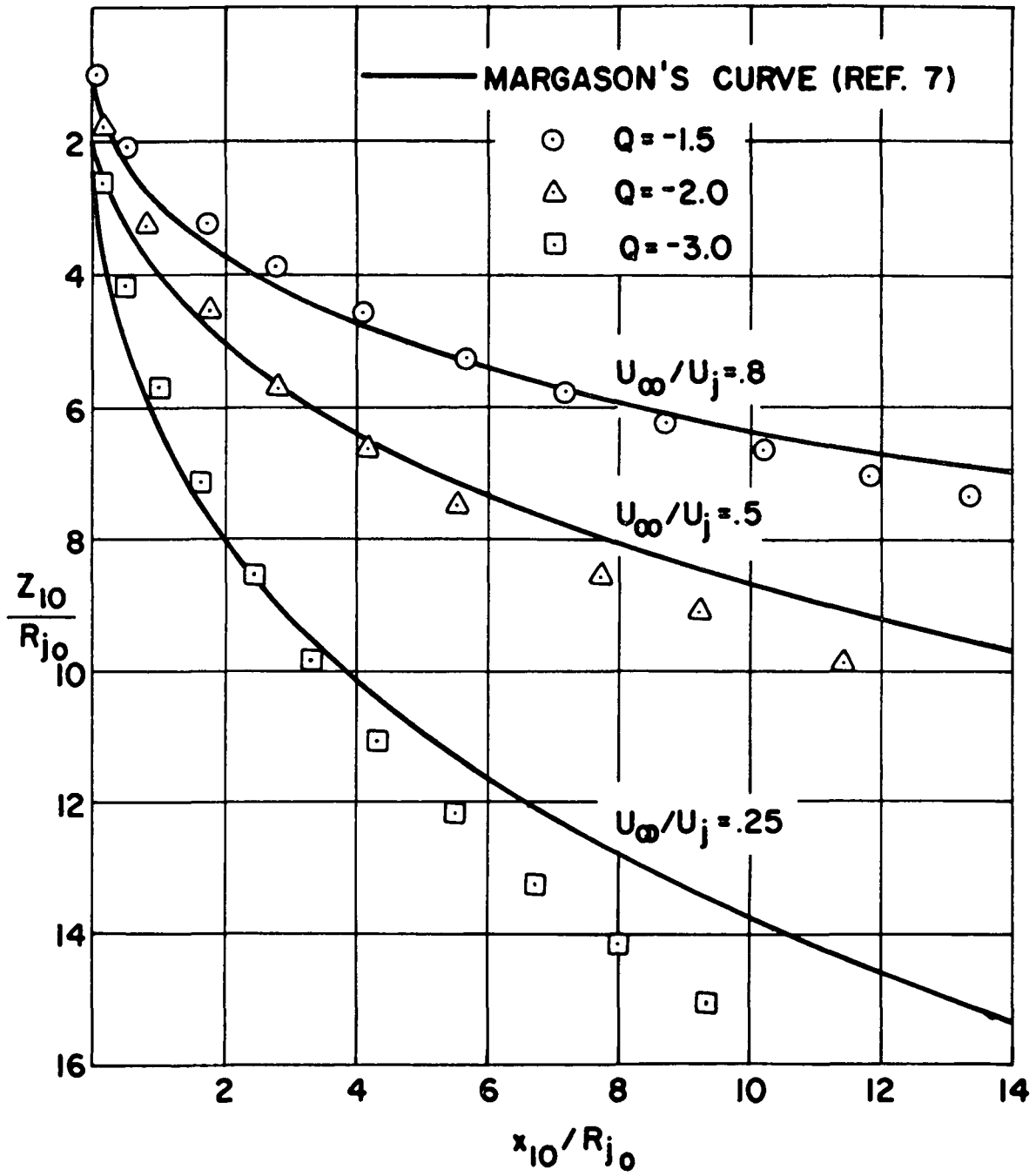

Fig. 12 - Jet Trajectory

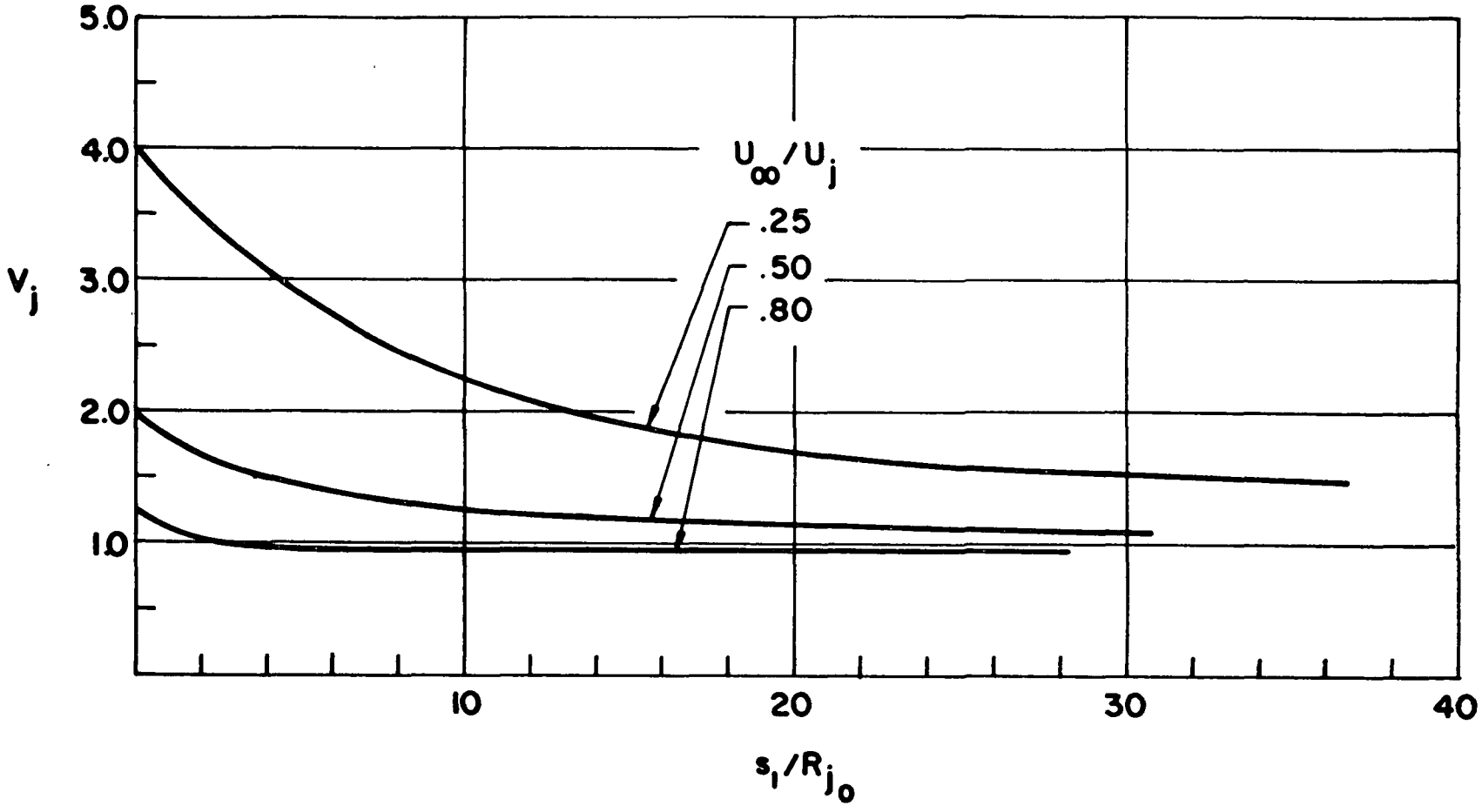

Fig. 13 - Jet Velocity V_j

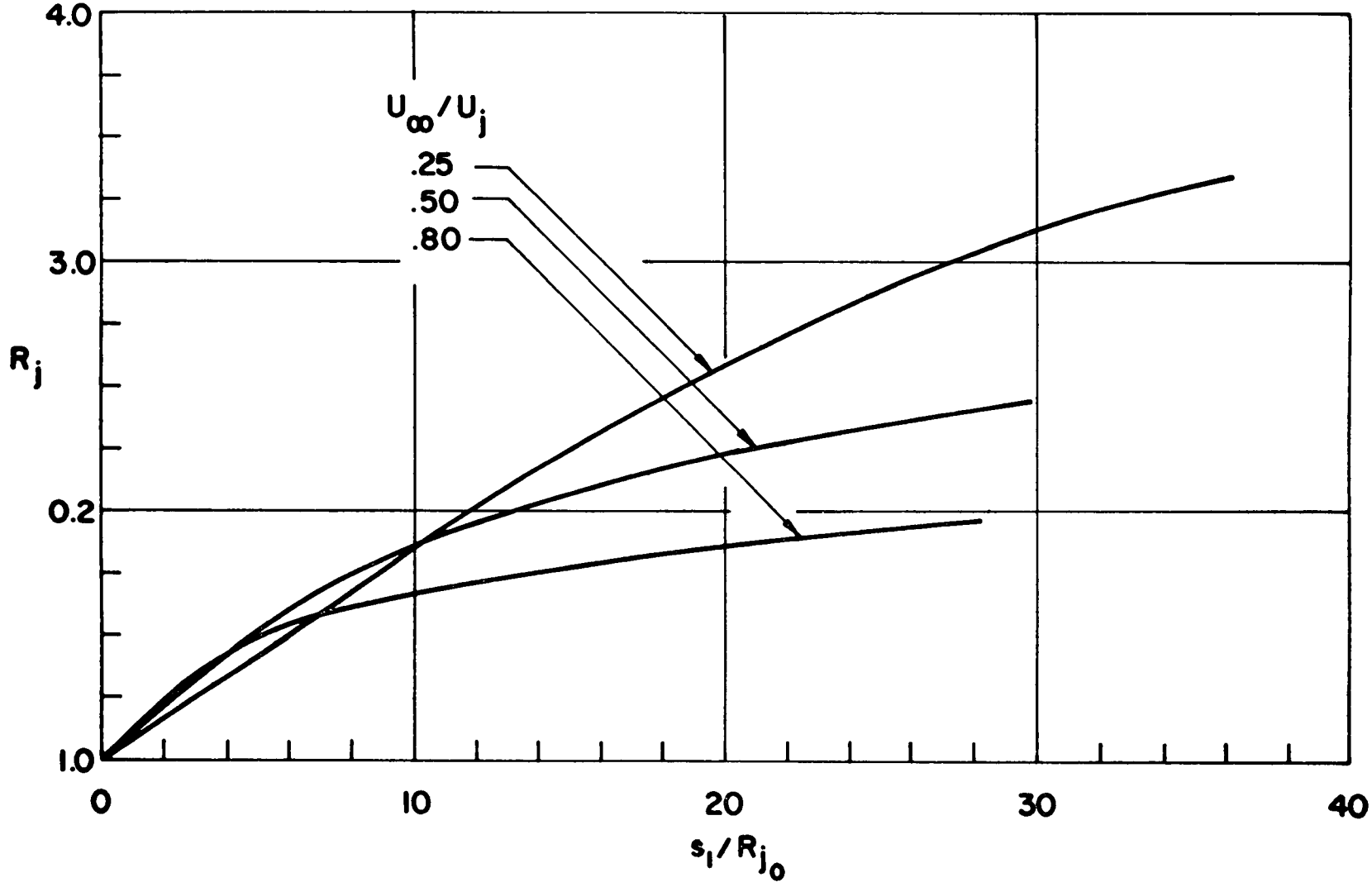

Fig. 14 - Jet Radius R_j

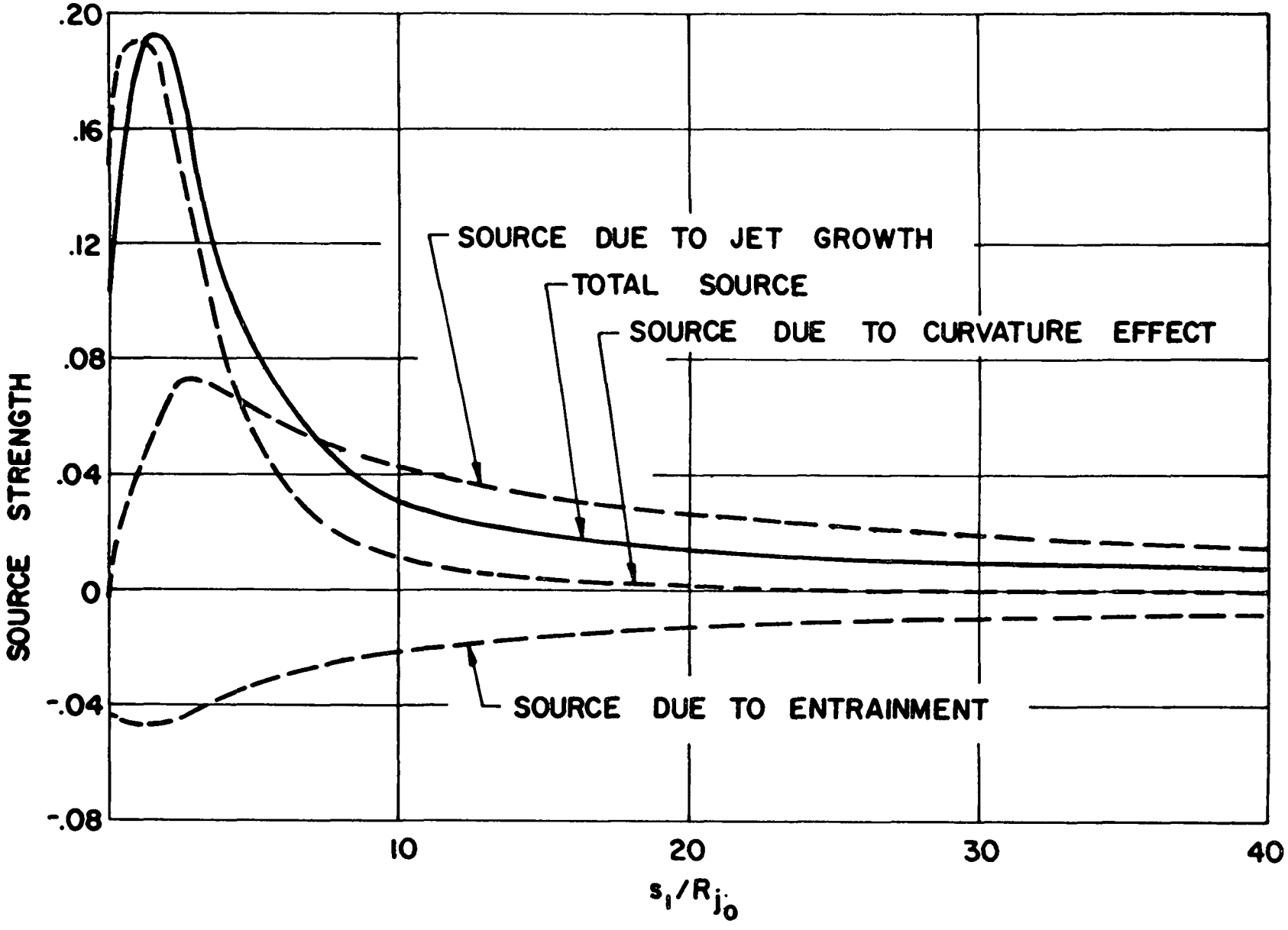

Fig. 15 - Comparison Of Source Strength Of Different Origin, $U_\infty/U_j = .8$

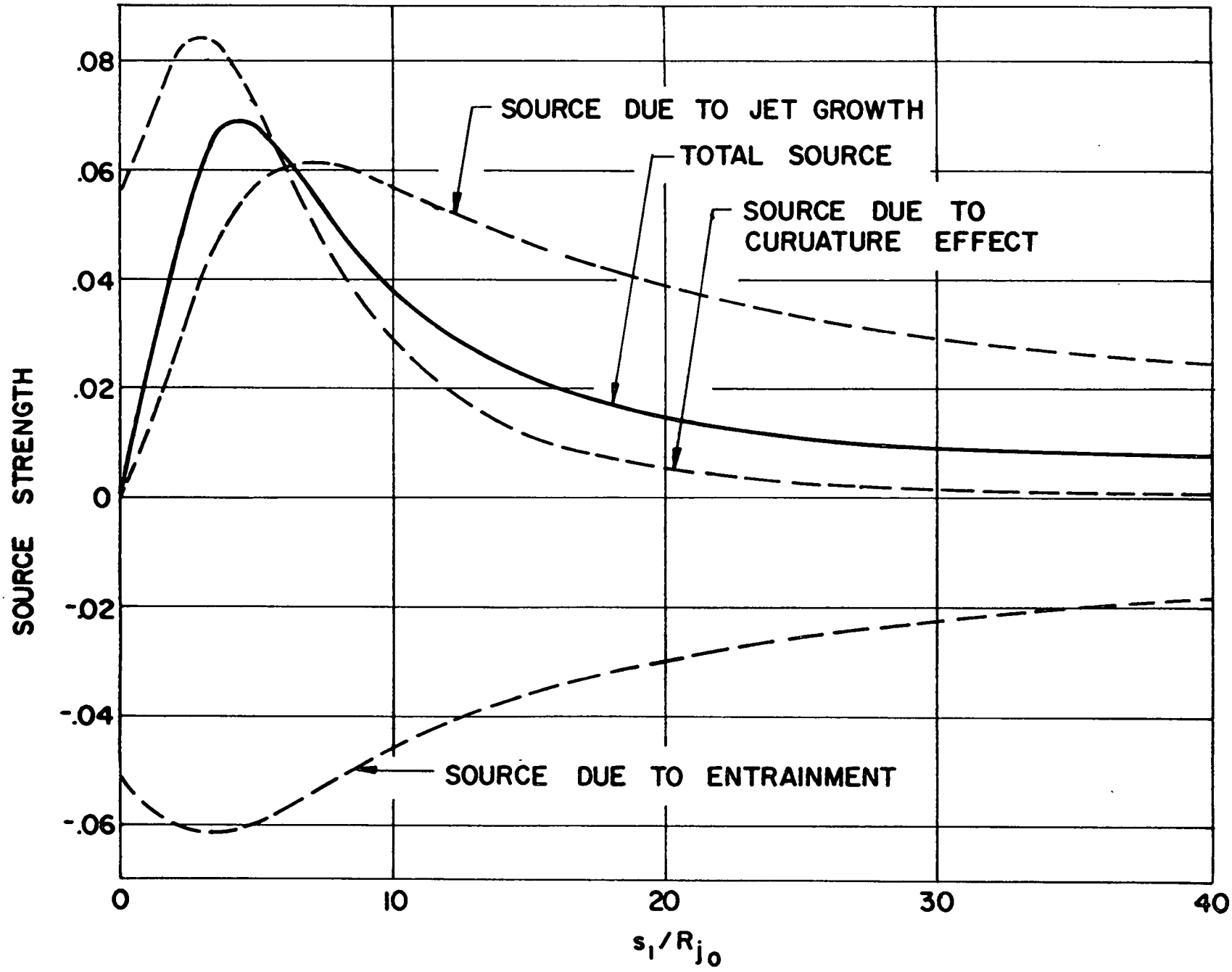

Fig. 16 - Comparison of Source Strength of Different Origin, $U_\infty/U_j = .5$

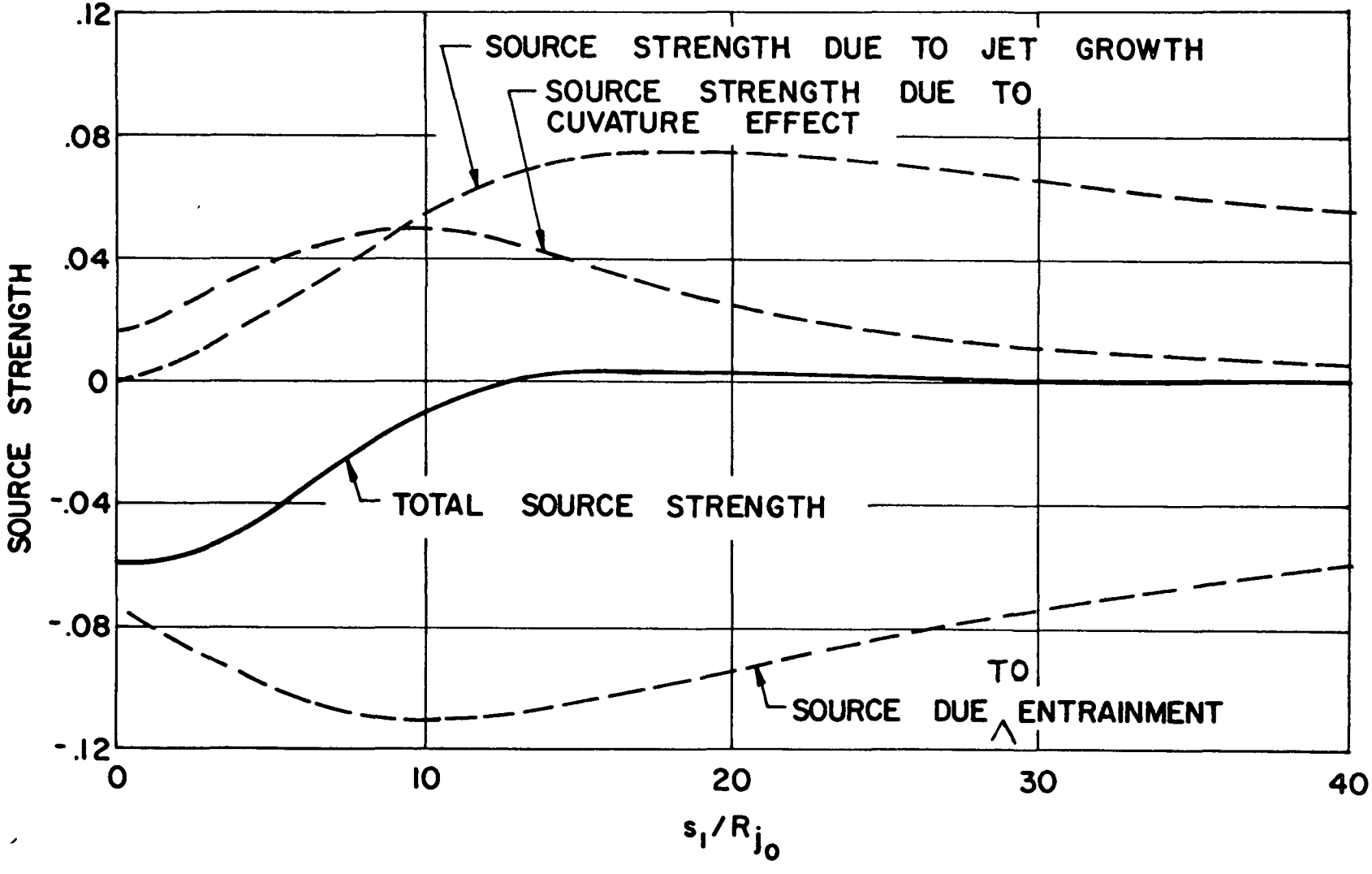

Fig. 17 - Comparison Of Source Strength Of Different Origin, $U_\infty/U_j = .25$

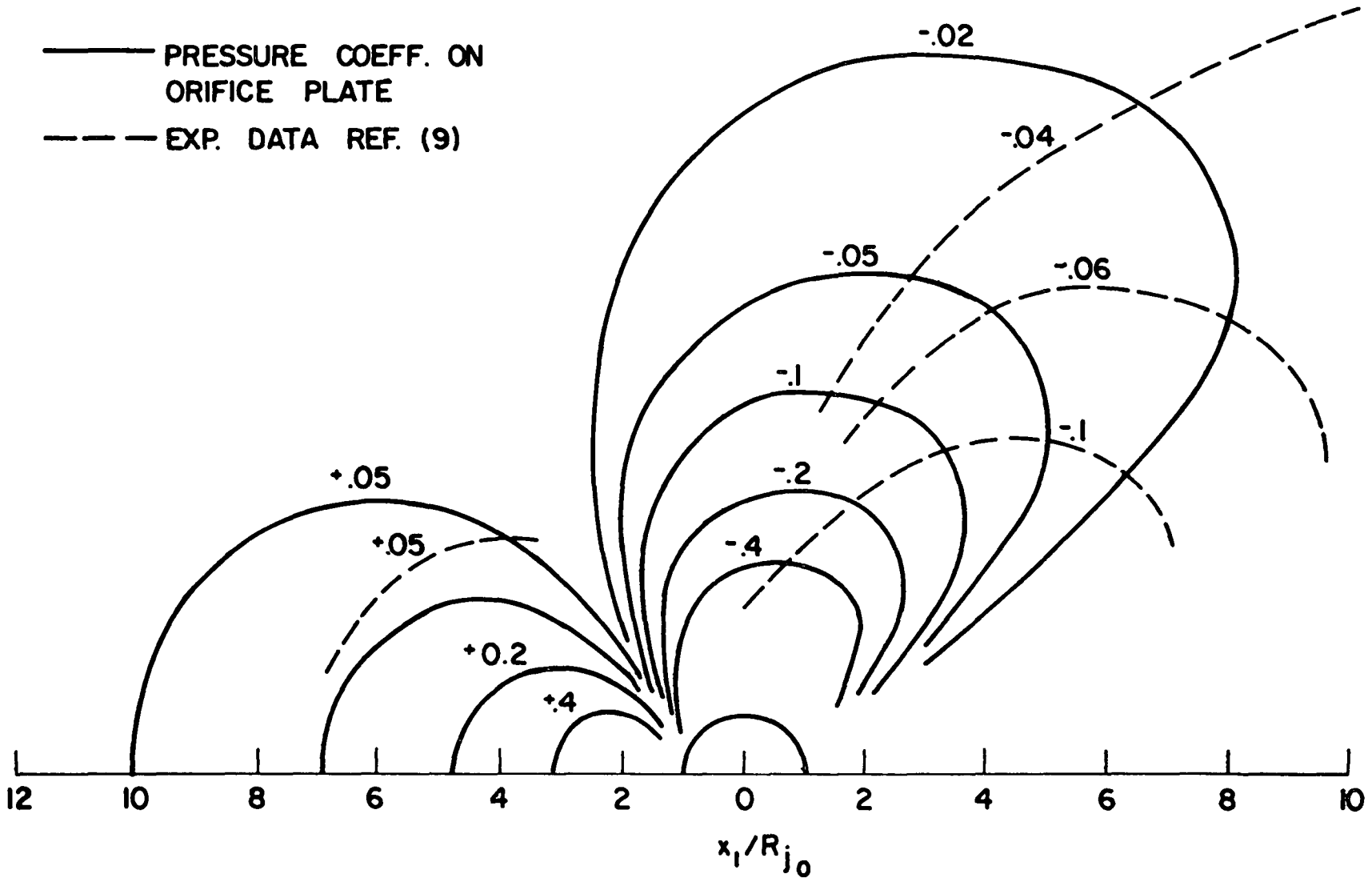

Fig. 18a - Pressure Contour, Outer Solution, U_∞/U_j = .8

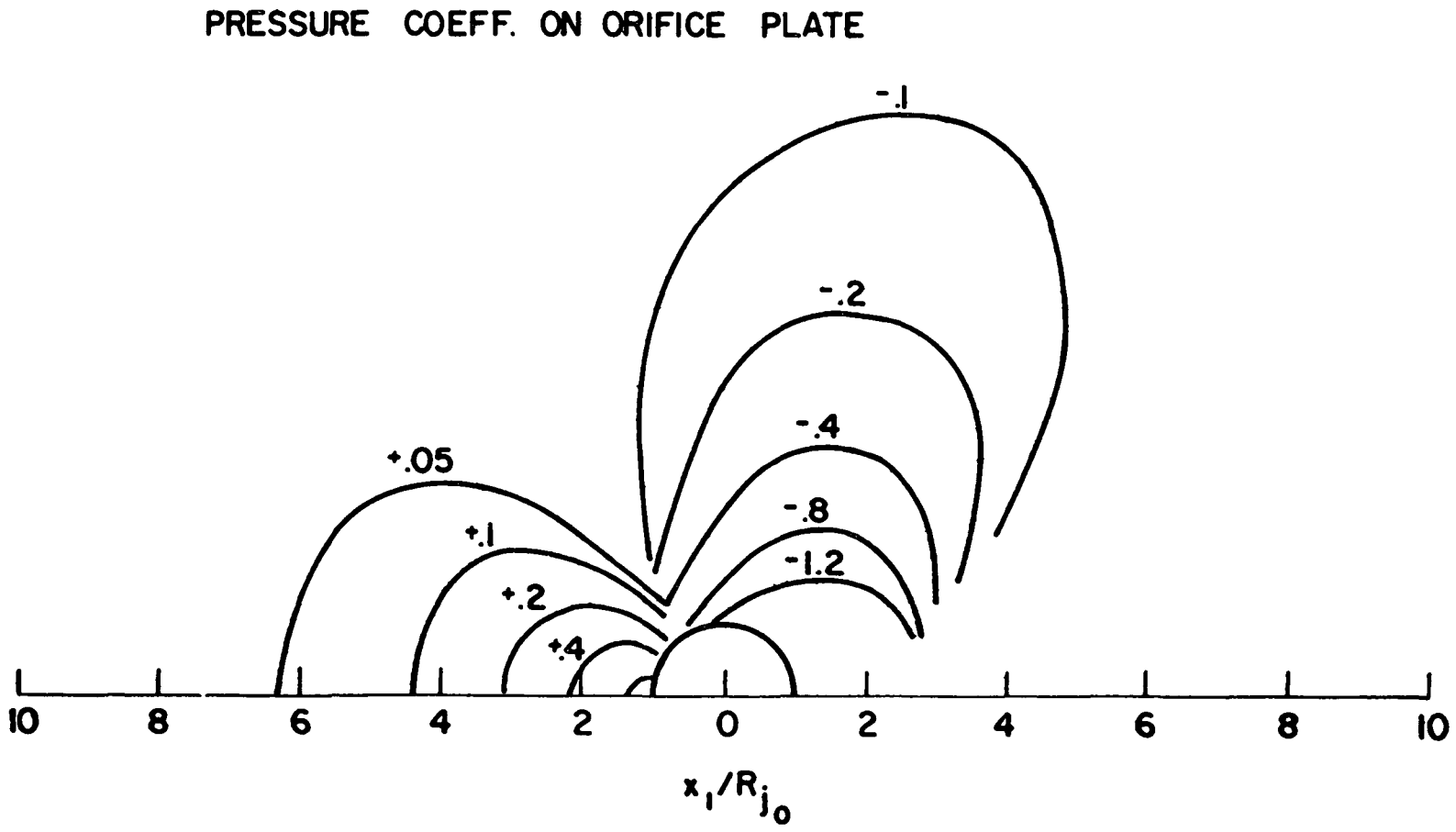

Fig. 18b - Pressure Contour, Inner Solution, $U_\infty/U_j = .8$

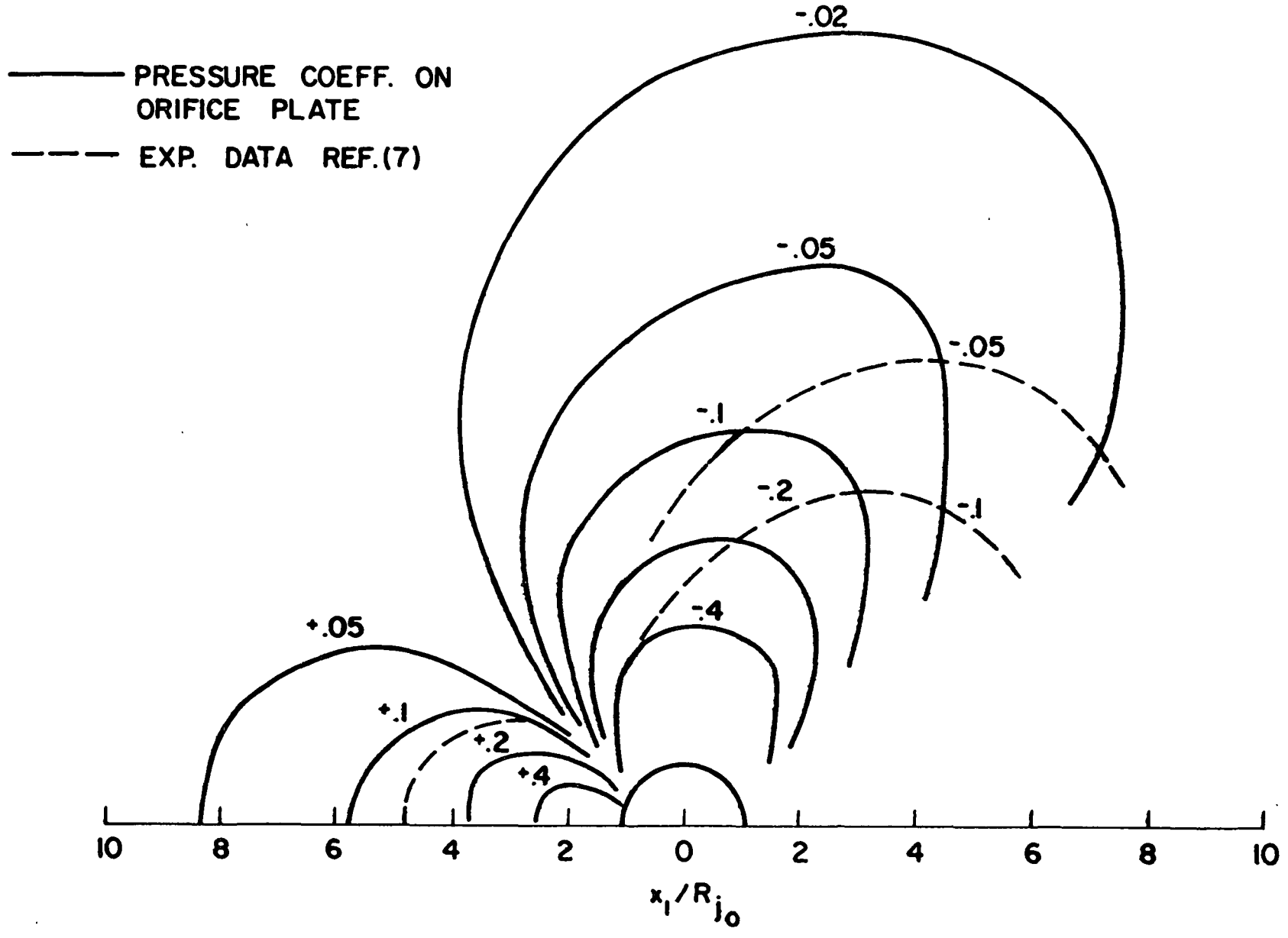

Fig. 19a - Pressure Contour, Outer Solution, U_∞/U_j = .5

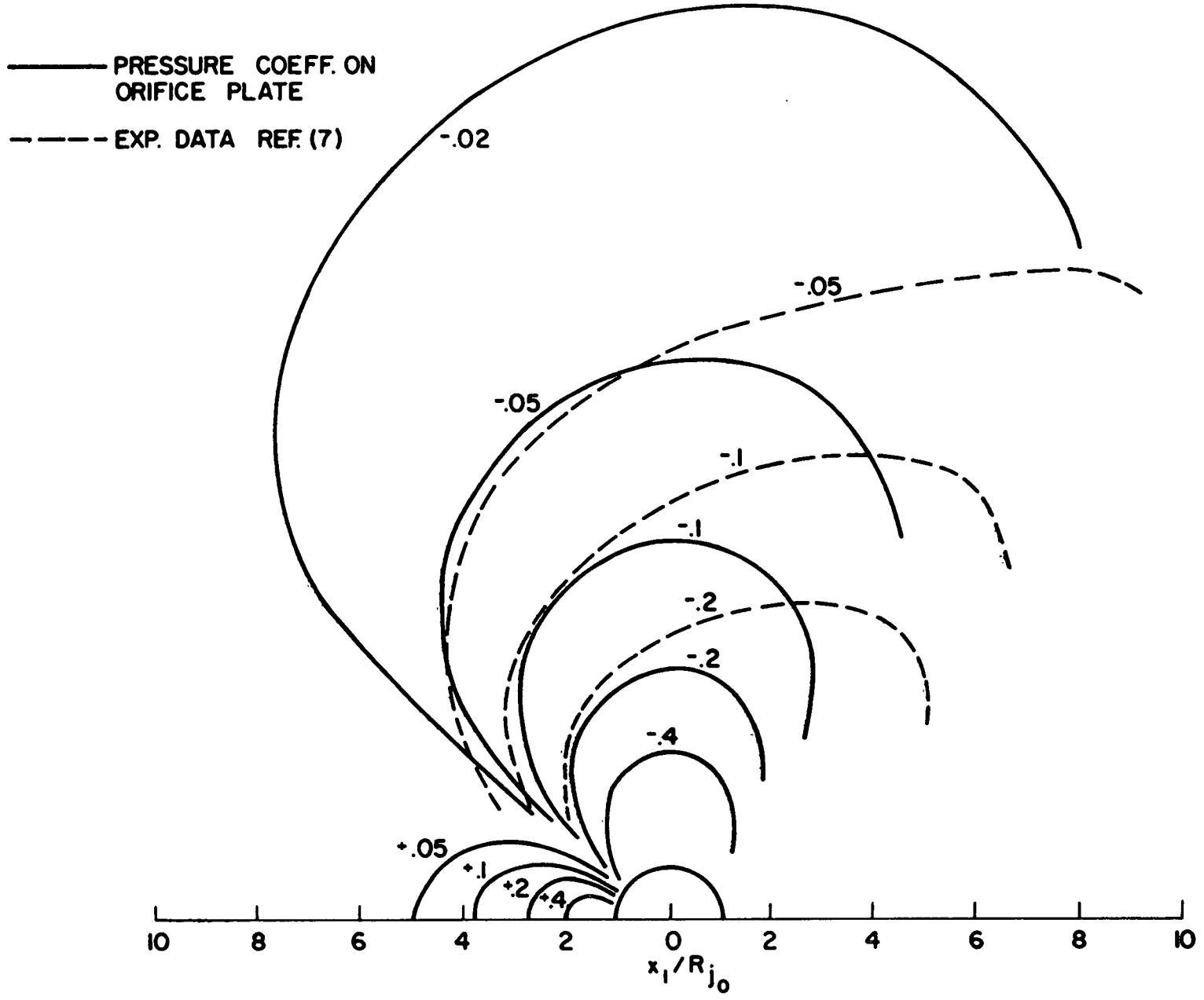

Fig. 20a - Pressure Contour, Outer Solution, U_∞/U_j = .25

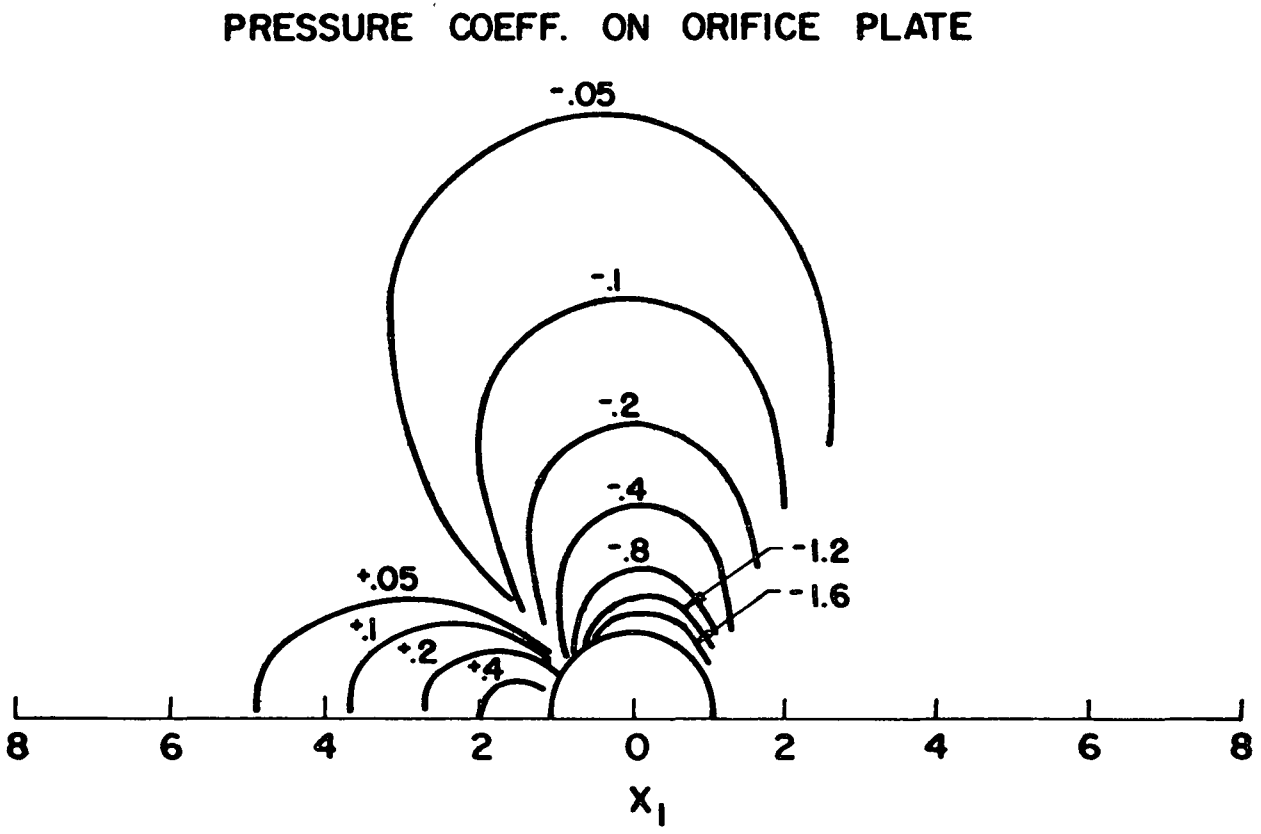

Fig. 20b - Pressure Contour, Inner Solution, U_∞/U_j = .25